國立交通大學

電機學院光電顯示科技產業研發碩士班

碩 士 論 文

流動引致分子排列之液晶繞射光柵

Liquid Crystal Diffraction Grating Made by Flow Induced Method

研 究 生：黃世民

指導教授：陳皇銘　教授

中 華 民 國 九 十 六 年 七 月

流動引致分子排列之液晶繞射光柵

Liquid Crystal Diffraction Grating Made by Flow Induced Method

研 究 生：黃世民　　　　Student：Shih-Min Huang

指導教授：陳皇銘　　　　Advisor：Huang-Ming Philip Chen

國 立 交 通 大 學

電機學院光電顯示科技產業研發碩士班

碩 士 論 文

A Thesis

Submitted to College of Electrical and Computer Engineering

National Chiao Tung University

in partial Fulfillment of the Requirements

for the Degree of

Master

in

Industrial Technology R & D Master Program on

Photonics and Display Technologies

July 2007

Hsinchu, Taiwan, Republic of China

中華民國九十六年七月

流動引致分子排列之液晶繞射光柵

學生：黃世民　　　　　　　　　　　　　　指導教授：陳皇銘 博士

國立交通大學電機學院產業研發碩士班

摘　　　要

　　液晶相位光柵具有分光、可調變特性，在光通訊、光譜儀甚至投影顯示系統等領域都被廣為使用，本論文提出一種別於傳統製作液晶光柵的作法，利用向列液晶自然流動時所呈現的物理特性，加上利用可聚合的光反應型液晶材料，達到不用配向層而能使液晶分子具有排列秩序，經光聚合反應後將液晶分子的排列鎖定，進而得到具有光學異向性的聚合物光柵。隨後在光柵中流入可隨電場驅動之液晶材料，即可得到一可調變繞射強度之液晶相位光柵。此種光柵可不受電場邊緣效應的影響，因而可大幅縮小光柵週期，進一步提升其可應用之範疇。

Liquid Crystal Diffraction Grating
Made by Flow Induced Method

Student：Shih-Min Huang   Advisors：Dr. Huang-Ming Philip Chen

Industrial Technology R & D Master Program of
Electrical and Computer Engineering College
National Chiao Tung University

ABSTRACT

Liquid crystal Diffraction Gratings can be applied for beam splitting and electrically tuning. It was widely used in optical communication, spectrometer and projection display technologies. In this thesis, a novel method different from the traditional fabrication is proposed. We made use of a photo-reactive mesogen and utilized the physic property of free flowing nematic liquid crystal. The molecular orientation without alignment layer was acquired. After photo-polymerization, the order of the orientation was locked. Anisotropic polymer gratings, then, were formed. The LC material that can be driven by electric fields was filled into the polymer grating and then a tunable LCPG was obtained. The Grating is free from the limitation caused by fringing field effect. Therefore, the period of grating can be reduced and the field of application will expand.

誌　　　謝

　　回想碩士生涯的點點滴滴，實在感觸良多，此篇論文得以順利完成，首先必須感謝我的指導教授-陳皇銘老師，因為老師孜孜不倦地教誨，讓我不僅僅在研究領域更上層樓，其認真嚴謹的態度，也讓我在為人處事上有長足的進步。

　　再者，我要感謝全實驗室的成員，因為有你們，讓我在交大的日子繽紛而多采，縱使研究的過程有苦有甘，你們的參與確實讓我覺得充實而不寂寞。謝謝昀諺、淇文、鴻杰學長，你們的經驗傳承與指正讓我獲益匪淺，謝謝宜揚、書豪兩位同窗好友，你們的協助及情誼著實讓我銘感五內，謝謝耀慶、文孚、尨綺、耿睿、威慶、佳恬、昆展、佑儒…等眾位學弟妹，有你們的幫忙，才有這美好的結果。此外，我也要感謝提供此一機會，讓我能在學問上深造的統寶光電公司及交通大學。

　　最後，要感謝栽培我至今的父母親及家人，您們無怨無悔的付出，才能造就現在的我，還要感謝吟珊，有妳的支持與陪伴，讓我在低潮時不會喪失鬥志，在歡欣鼓舞時能獲得分享的喜悅。

　　感謝全能的天父，祢賜磨練予我，讓我學習謙卑，賜平安予我，讓我懂得恭順，賜喜樂予我，讓我明白感恩，我要將榮耀歸您，並將此文獻給所有我感激的人。

Table of contents

List of Figures

List of Tables

Chapter 1

Introduction

1.1 Diffractive Optical Elements

Diffractive optical elements (DOEs) [1] make use of the diffraction of electromagnetic waves at structured materials. Depending on the ratio of the period of the structure Λ to the wavelength λ of the electromagnetic radiation quite different optical properties like anti-reflection, spectrally filtering, light trapping or light distribution and re -direction can be achieved (see Table 1.1). So far, most of the applications of diffractive optical elements in telecommunication, imaging, lighting and security devices required DOEs on relatively small areas.
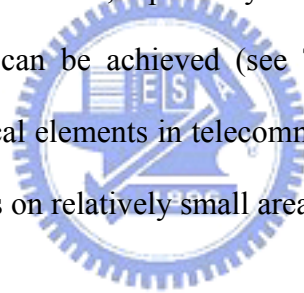
Tab. 1.1 The different application of diffractive optical elements

Period to wavelength ratio	Applications
$\Lambda \ll \lambda$	anti-reflective surfaces, polarizers, retarders, selective radiation emitters
$\Lambda \cong \lambda$	filters, small-bandwidth selective radiation emitters
$\Lambda \gg \lambda$	light steering elements, retro-reflectors, concentrators

In recent years, DOEs have been widely used in various optical systems. Because of its small size, light weight, great versatility, and low cost, DOEs become the first choice for laser beam shaping and focusing [2], spectral synthesizing, laser coupling, correlation filtering, wavelength-division multiplexing, signal processing, optical disk reading out, beam array generating, and so on. Flexible spectrum synthesis now plays an important role in optical communication system for all optical network.

1.2 Liquid Crystal

Liquid crystals [3][4] are substances that exhibit a phase of matter that has properties between those of a conventional liquid, and those of a solid crystal. For instance, a liquid crystal (LC) may flow like a liquid, but have the molecules in the liquid arranged or oriented in a crystal-like way [5]. There are many different types of LC phases, which can be distinguished based on their different optical properties (such as birefringence). When viewed under a microscope using a polarized light source, different liquid crystal phases will appear to have a distinct texture [6]. Each "patch" in the texture corresponds to a domain where the LC molecules are oriented in a different direction. Within a domain, however, the molecules are well ordered. Liquid crystal materials may not always be in an LC phase. Liquid crystals can be divided into thermotropic and lyotropic LCs. Thermotropic LCs exhibit a phase transition into the LC phase as temperature is changed, whereas lyotropic LCs exhibit phase transitions as a function of concentration of the mesogen in a solvent as well as temperature. Fig 1.1 shows the typical phase transition in thermotropic liquid crystals.
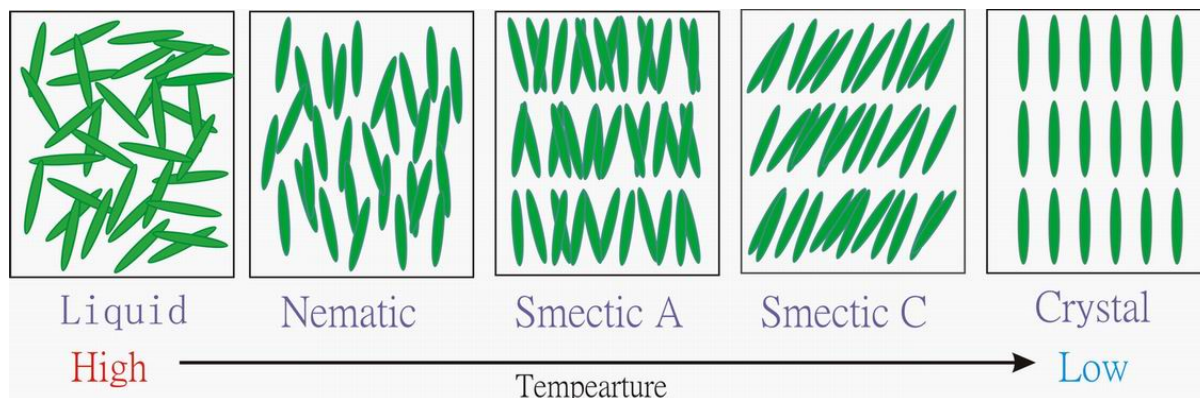
Fig. 1.1 Structures of some typical phases from high temperature to low temperature in thermotropic liquid crystals.

1.2.1 Liquid Crystal Phases

The liquid crystal state is a distinct phase of matter observed between the crystalline (solid) and isotropic (liquid) states. There are many types of liquid crystal states, depending upon the amount of order in the material. This section will explain the common phase behavior of liquid crystal materials.

Nematic phases

Nematic liquid crystals are subdivided into the ordinary nematic and the chiral-nematic (or cholesteric). The molecules in the ordinary nematic structure maintain a parallel or nearly parallel arrangement to each other along the long molecular axes. They are mobile in three directions and can rotate about one axis. This structure is one-dimensional. Fig. 1.2 displays the diagram of nematic and cholesteric liquid crystals.

When the nematic structure is heated, it is generally transformed into the isotropic liquid where the completely disordered motion of the molecules produces a phase in

which all directions are equivalent. The nematic structure is the highest-temperature mesophase in thermotropic liquid crystals. The energy required to deform a nematic liquid crystal is so small that even the slightest perturbation caused by a dust particle can distort the structure considerably.

(a)   (b)   (c)

Fig. 1.2 The molecular arrangement of (a) nematic (b), (c) chiral-nematic phases.
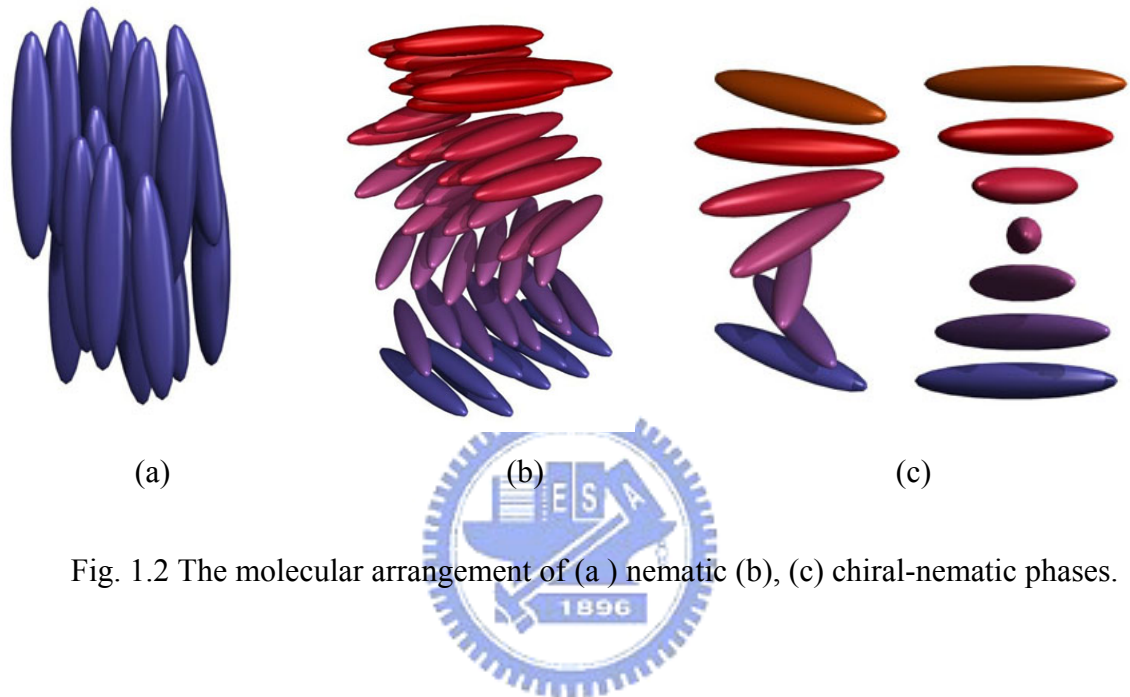
Smectic phases

The word "smectic" is derived from the Greek word for soap. This seemingly ambiguous origin is explained by the fact that the thick, slippery substance often found at the bottom of a soap dish is actually a type of smectic liquid crystal.

The smectic state is another distinct mesophase of liquid crystal substances. Molecules in this phase show a degree of translational order not present in the nematic. In the smectic state, the molecules maintain the general orientational order of nematics, but also tend to align themselves in layers or planes. Motion is restricted to within these

planes, and separate planes are observed to flow past each other. The increased order means that the smectic state is more "solid-like" than the nematic.

Many compounds are observed to form more than one type of smectic phase. As many as 12 of these variations have been identified, however only the most distinct phases are discussed here.

In the smectic-A mesophase, the director is perpendicular to the smectic plane, and there is no particular positional order in the layer. Similarly, the smectic-B mesophase orients with the director perpendicular to the smectic plane, but the molecules are arranged into a network of hexagons within the layer. In the smectic-C mesophase, molecules are arranged as in the smectic-A mesophase, but the director is at a constant tilt angle measured normally to the smectic plane.

As in the nematic, the smectic-C mesophase has a chiral state designated C*. Consistent with the smectic-C, the director makes a tilt angle with respect to the smectic layer. The difference is that this angle rotates from layer to layer forming a helix. In other words, the director of the smectic-C* mesophase is not parallel or perpendicular to the layers, and it rotates from one layer to the next. Fig.1.3 present the diagrams of three kinds of sematic phases.
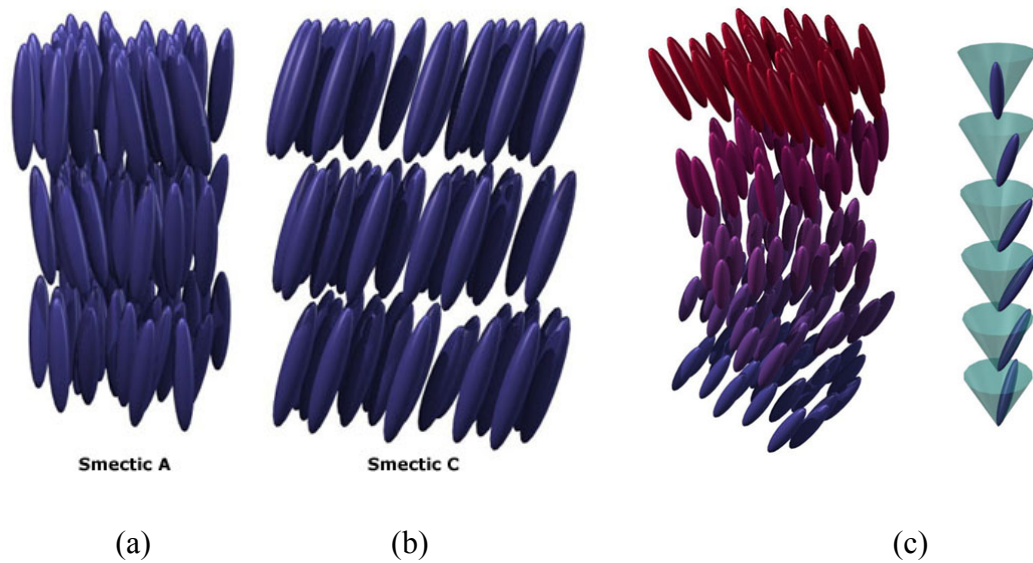
Fig. 1.3 The molecular arrangement of (a) sematic-A, (b) sematic-C and (c) sematic-C* phases.

Cholesteric Phases

The cholesteric (or chiral nematic) liquid crystal phase is typically composed of nematic mesogenic molecules containing a chiral center which produces intermolecular forces that favor alignment between molecules at a slight angle to one another. This leads to the formation of a structure which can be visualized as a stack of very thin 2-D nematic-like layers with the director in each layer twisted with respect to those above and below. In this structure, the directors actually form in a continuous helical pattern about the layer normal as illustrated by the black arrow in the following figure and animation. The black arrow in the animation represents director orientation in the succession of layers along the stack.

The molecules shown are merely representations of the many chiral nematic mesogens lying in the slabs of infinitesimal thickness with a distribution of orientation around the director. This is not to be confused with the planar arrangement found in smectic mesophases.

(a)

(b)
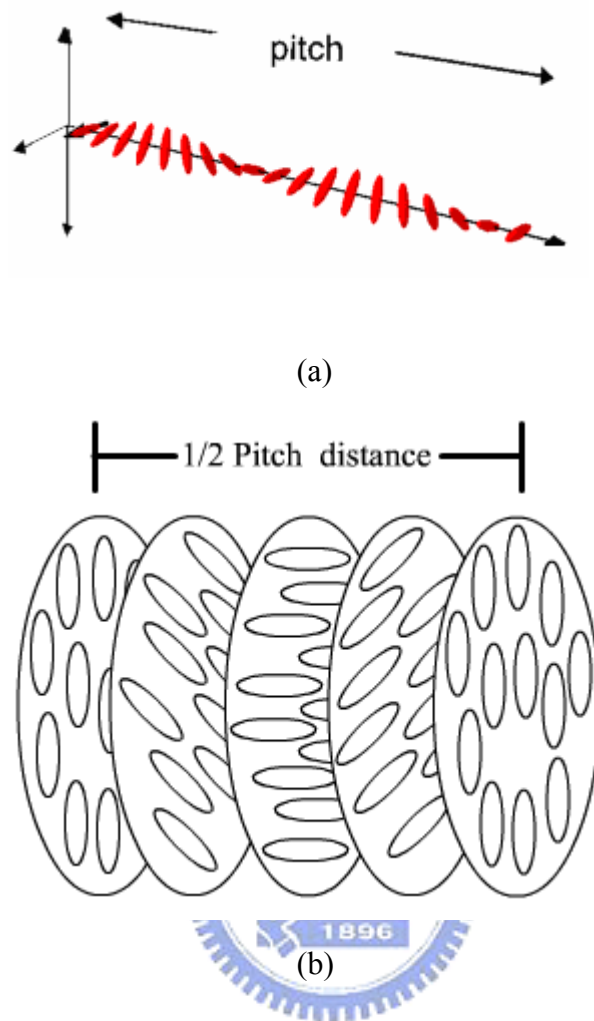
Fig. 1.4 (a) The pitch of the cholesteric mesophase. (b) The gradual change in
director orientation between successive layers

An important characteristic of the cholesteric mesophase is the pitch. The pitch, p,
is defined as the distance it takes for the director to rotate one full turn in the helix as
illustrated in the above animation. A byproduct of the helical structure of the chiral
nematic phase, is its ability to selectively reflect light of wavelengths equal to the pitch
length, so that a color will be reflected when the pitch is equal to the corresponding
wavelength of light in the visible spectrum. The effect is based on the temperature
dependence of the gradual change in director orientation between successive layers
(illustrated in Fig. 1.4), which modifies the pitch length resulting in an alteration of the

wavelength of reflected light according to the temperature. The angle at which the director changes can be made larger, and thus tighten the pitch, by increasing the temperature of the molecules, hence giving them more thermal energy. Similarly, decreasing the temperature of the molecules increases the pitch length of the chiral nematic liquid crystal. This makes it possible to build a liquid crystal thermometer that displays the temperature of its environment by the reflected color. Mixtures of various types of these liquid crystals are often used to create sensors with a wide variety of responses to temperature change. Such sensors are used for thermometers often in the form of heat sensitive films to detect flaws in circuit board connections, fluid flow patterns, condition of batteries, the presence of radiation, or in novelties such as "mood" rings.

In the fabrication of films, since putting chiral nematic liquid crystals directly on a black background would lead to degradation and perhaps contamination, the crystals are micro-encapsulated into particles of very small dimensions. The particles are then treated with a binding material that will contract upon curing so as to flatten the microcapsules and produce the best alignment for brighter colors. An application of a class of chiral nematic liquid crystals which are less temperature sensitive is to create materials such as clothing, dolls, inks and paints.

The wavelength of the reflected light can also be controlled by adjusting the chemical composition, since cholesterics can either consist of exclusively chiral molecules or of nematic molecules with a chiral dopant dispersed throughout. In this case, the dopant concentration is used to adjust the chirality and thus the pitch.

Isotropic Phase

In the isotropic phase the moelcules are randomly aligned and exhibit no long range order.

The isotropic phase has a low viscosity and will often appear to be crystal clear. There is no long range positional or orientational order of the molecules, although this sort of order may exist on very short length scales of order tens of Angstroms, corresponding to a few molecular distances. For all practical purposes, the isotropic phase macroscopically appears to be like any other isotropic liquid such as water.

1.2.2 Order parameter

To quantify just how much order is present in a material, an order parameter (S) is defined. Traditionally, the order parameter is given as Fig.1.5:
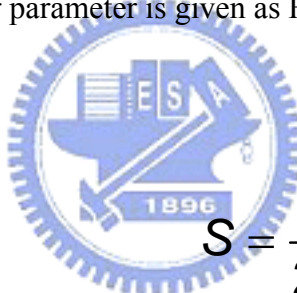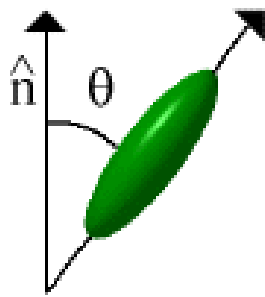
$$S = \frac{1}{2}\left\langle 3\cos^2\theta - 1 \right\rangle$$

(1.1)

Fig.1.5 Definition of the nematic director, n and order parameter.

where theta is the angle between the director and the long axis of each molecule. The brackets denote an average over all of the molecules in the sample. In an isotropic liquid, the average of the cosine terms is zero, and therefore the order parameter is equal to zero. For a perfect crystal, the order parameter evaluates to one [7]. Typical values for the order parameter of a liquid crystal range between 0.3 and 0.9, with the exact value a function of temperature, as a result of kinetic molecular motion.

1.2.3 Liquid Crystal Anisotropy

The essential properties of a liquid crystal are its optical and electromagnetic anisotropy. Optical anisotropy [8] means that the index of refraction of the material depends on the direction of light polarization. One describes the optical properties of the LC by the so-called indicatrix, which is an ellipsoid with its long/short axis equal to the index of refraction parallel $n_{\parallel}$ or perpendicular $n_{\perp}$ to the optic axis. The difference $\Delta n = n_{\parallel} - n_{\perp}$ is called birefringence [9]. In principle optically positive materials (like N, SmA) have $\Delta n > 0$. The reverse is true for optically negative materials. Fig.1.6 (a) shows an indicatrix of positive and negative medium in a uniaxial phase, with two principal refractive indices and only one optic axis. The optic axis is defined as the normal to the plane whose intersection with the indicatrix is a circle. There exist materials characterized by three principal refractive indices: n_1, n_2 and n_3 referred to as a medium with biaxial phase (like SmC). The indicatrix becomes a flattened ellipsoid because the material exhibits two optic axes. Fig.1.6 (b) presents a typical indicatrix with $n_1 < n_2 < n_3$, usually found in ferroelectric materials. The difference $\delta n = n_2 - n_1$ is called optical biaxiality. Since the biaxiality of liquid crystals is very small ($n_1 \approx n_2$), it is very often neglected for simplicity. Although the indicatrix has an ellipsoidal shape, it is not related to the elongated shape of the molecule and should not be confused.

(a)   (b)
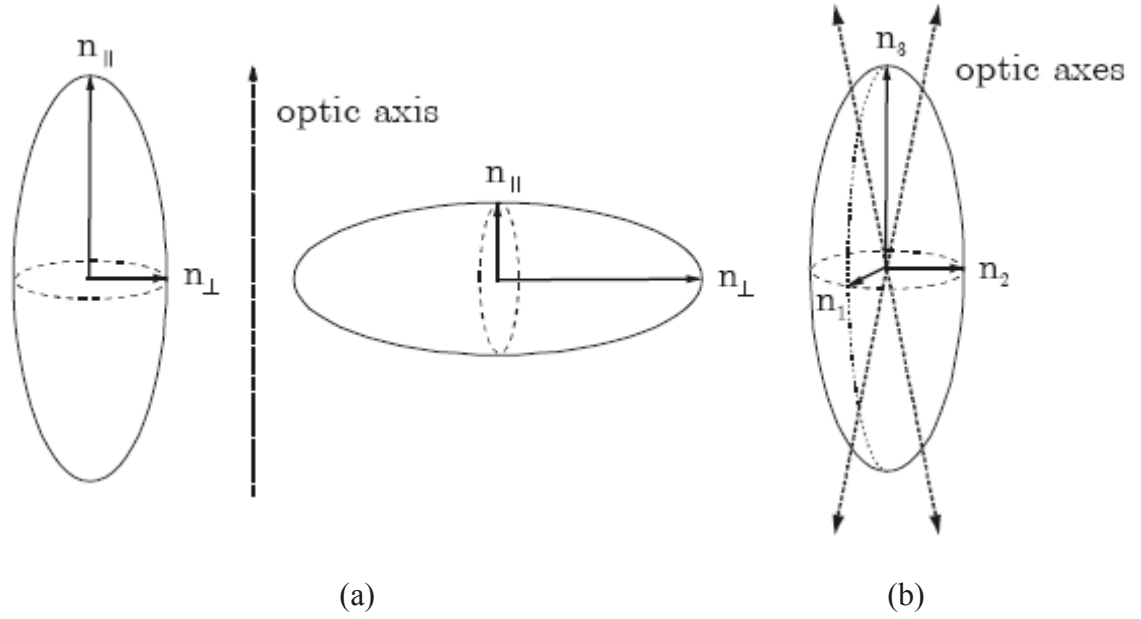
Fig. 1.6 Illustration of the optical indicatrix of (a) uniaxial and (b) optically

positive biaxial material.

A light beam entering the liquid crystal layer, is split into two components: the

ordinary and extraordinary ray. Both rays propagate through the birefringent medium at

different velocities, because they experience different indices of refraction, n_o and n_e.

These are related to the principal indices of refraction $n_\parallel$ and $n_\perp$ by:

$$n_0 = n_\perp \quad \text{and} \quad n_e = \frac{n_\parallel n_\perp}{\sqrt{n_\parallel^2 \cos^2 \phi_0 + n_\perp^2 \sin^2 \phi_0}}$$

(1.2)

with $\Phi 0$ being the angle between the optic axis and the direction of light propagation.

Different ray velocities lead to a phase difference Λ at the output of the liquid crystal

layer, which is defined by:

$$\Lambda = \frac{2\pi}{\lambda}(n_e - n_o)d$$

(1.3)

where λ is the wavelength of light (in vacuum) and d is the distance across the

homogeneous LC layer (for normal incidence this is equal to the cell gap).

In order to calculate the transmission through a LC layer one has to start with

linearly polarized incident light (polarizer P), which is converted by the medium to

elliptically polarized light, with only a fraction which is able to pass through the analyzer (A), oriented at 90° with respect to the polarizer. For that case the transmitted intensity is given by the formula:

$$I = I_0 \sin^2 2\alpha \sin^2 \frac{\Lambda}{2}$$

(1.4)

where I_0 is the intensity of the linearly polarized light, α is the angle between the polarizer and the optic axis of the medium and Λ is the phase difference between the incoming and outcoming wave. This simple formula is the basis for more powerful simulation packages for optical calculations (Berreman formalism, Jones calculus), taking into account oblique incidence, reflections and other [10][11].
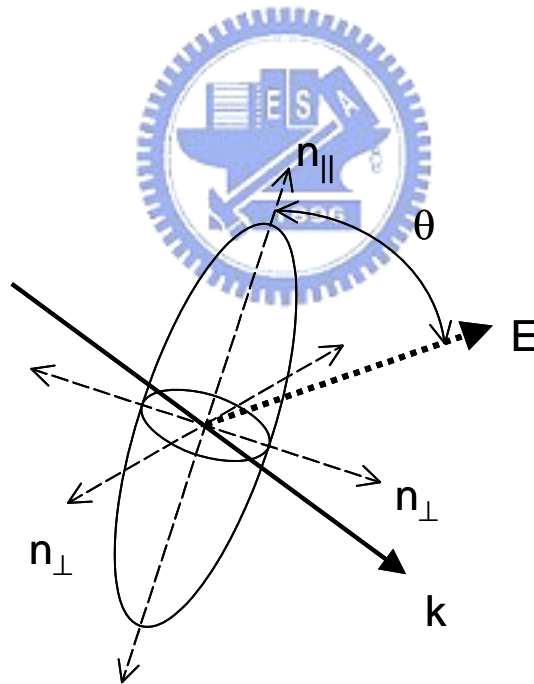
Fig.1.7 Refractive indices of a uniaxial nematic liquid crystal molecule in an appliedelectric field.

As mentioned earlier, liquid crystals exhibit shape anisotropy, which gives them their unique phase ordering properties. This shape anisotropy manifests itself in other physical properties of the material such as the dielectric constant, index of refraction, and magnetic susceptibility. Consider a uniaxial nematic liquid crystal in an applied electric field, E, as in Fig.1.7. The field will polarize the spatial charge distribution within the molecule, inducing a dipole moment, P [12]. The induced dipole moment is proportional to the electric field as long as the field is not too large:

$$P = \varepsilon_0 \chi_e E \tag{1.5}$$

where $\varepsilon_0 = 8.85 \times 10^{-12}$ C^2/Nm^2 is the permittivity of free space and χ_e is the electric susceptibility. Due to the shape anisotropy of the liquid crystal molecule, the electric susceptibility has one value when the electric field is applied parallel ($\chi_\parallel$) to the to the nematic director and a different value when applied perpendicular ($\chi_\perp$). The difference between these two values is

$$\Delta\chi = \chi_\parallel - \chi_\perp \tag{1.6}$$

which is often expressed as the dielectric anisotropy

$$\Delta\varepsilon = \varepsilon_\parallel - \varepsilon_\perp \tag{1.7}$$

where $\varepsilon = 1+\chi$, and $\varepsilon_\parallel$, $\varepsilon_\perp$ are the dielectric permittivities parallel and perpendicular to the molecular symmetry axis, respectively. The induced dipole moment will serve to reorient the nematic director such that its symmetry axis is parallel to the applied field direction ($\Delta\varepsilon > 0$, as with most materials) or perpendicular to the applied field direction ($\Delta\varepsilon < 0$). An analogous property holds true for magnetic susceptibilities also, however the fields necessary to achieve the molecular reorientation are too high for most practical devices.
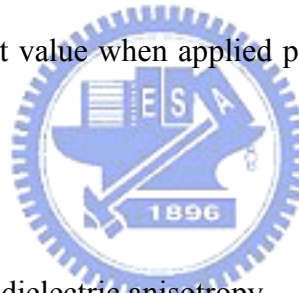
1.3 Liquid Crystal Diffraction Gratings

In recent years, electrically tunable diffraction gratings are of interest for a number of optical and photonic applications. Liquid crystals are the materials of choice for fabricating such grating devices, and are actually applied to light modulators [13][14] and [15], display devices [16] and [17], beam steering [18] and [19], optical computing [20] and etc. The control of the diffraction efficiency is easily possible due to altering the LC alignment state or texture by applying external stimuli (ex. electric field and magnetic field, etc.). The LC gratings have been developed in various ways such as patterned electrodes [18] and [21], patterned alignment layers [16], [17]and [22], LC-filled periodic grooves [23] and LC-monomer mixtures [24], [25] and [26]. An easy fabrication [27] and [28] and reliability are indispensable to practical application for efficient devices. Moreover, the diffraction performance independent of incident polarization is desirable to increase the optical efficiency. Generally speaking, patterned electrodes, pattern alignment layers and holographic polymer-dispersed liquid crystal (H-PDLC) are the major fabrication methods of LC gratings.

1.4 Motivation and objective

The former processes of fabricating liquid crystal diffractive grating are widely reported. To make use of the electro optical property of liquid crystal, to overcome the present bottleneck of LC gratings and decrease the cost of manufacture, a method of fabricating polymer gratings in diffractive device is required in electro-optical industry.

As a result, the main objective of this thesis is to propose a novel fabrication method of polymer grating structures based on nature flowing properties of nematic

liquid crystal. This new process has the benefits of larger diffraction angle, no phase separation issue and no fringing field effect, besides it has great potential to develop a alignmentless LC device. The main concept of this design to fabricate the polymer grating is built on the lithography technology. Besides, the discussion of the results will also be given in this thesis.

1.5 Content of the Thesis

The thesis contributes to the research on the free flowing nematic phase of reactive mesogen and its application in the liquid crystal diffraction grating. Chapter 1 contains an introduction to diffractive optical elements and liquid crystals. It describes various liquid crystal phases and their basic physical properties and introduces the problem of each type of grating. Chapter 2 illustrates the operating principle of a conventional binary phase LC gratings configuration and its applications. It explains the mechanism of switching. The concept of reactive mesogen and flow alignment phenomenon were also discussed. Chapter 3 presents the fabrication method, the proposed model concepts which enable the molecular orientation without traditional alignment layer and the instruments used to verify experiment results. In Chapter 4 the result of our experiment are described by parts. In the case of the free flowing model, molecular alignment is presented, giving a natural self assembly property of nematic phase in flowing behavior. The last section of Chapter 4 contains a discussion of the method we reports, which will compare with the other proposed methods. Chapter 5 sums up the conclusions of this research work and future works.

Chapter 2

Fundamental Theory

2.1 Reactive Mesogen (RM)

Reactive mesogens are liquid crystalline materials with polymerizable end groups. Polymerization of reactive mesogens with two or more polymerizable groups leads to densely crosslinked networks in which the liquid crystalline order is permanently fixed [29]. The principle of this procedure is outlined in Fig.2.1.

In situ photo-initiated polymerization of the end groups in the liquid crystal phase allows the attainment of the optimum mesophase morphology and alignment, followed by the ''freezing in'' of this structure on creation of the crosslinked network shown. The formation of large area, monodomain, aligned morphology on cooling from the clearing point is possible due to the relatively low viscosity of these small molecules (in comparison to the analogous polymer systems which are more viscous) in the liquid crystalline phases.

This class of materials is attractive for a number of applications. For example cholesteric polymer networks from reactive mesogens are used as color flop pigments with a distinct viewing angle dependence of the color [30]. A second application of crosslinked cholesteric mesophases are broad band polarizers [31]. In such polarizers the reflected light is ''recycled'' and transmission up to 82% have been achieved. Another advantage of the use of reactive mesogens is that through the use of a shadow mask during the crosslinking process, pattern formation like in a negative photoresist is

possible. By using a sequence of photoisomerization and photopolymerization reactions Lub et al. produced a color filter for all three fundamental colors with a pixel size of 100 mm, which can be used in liquid crystal displays [32].
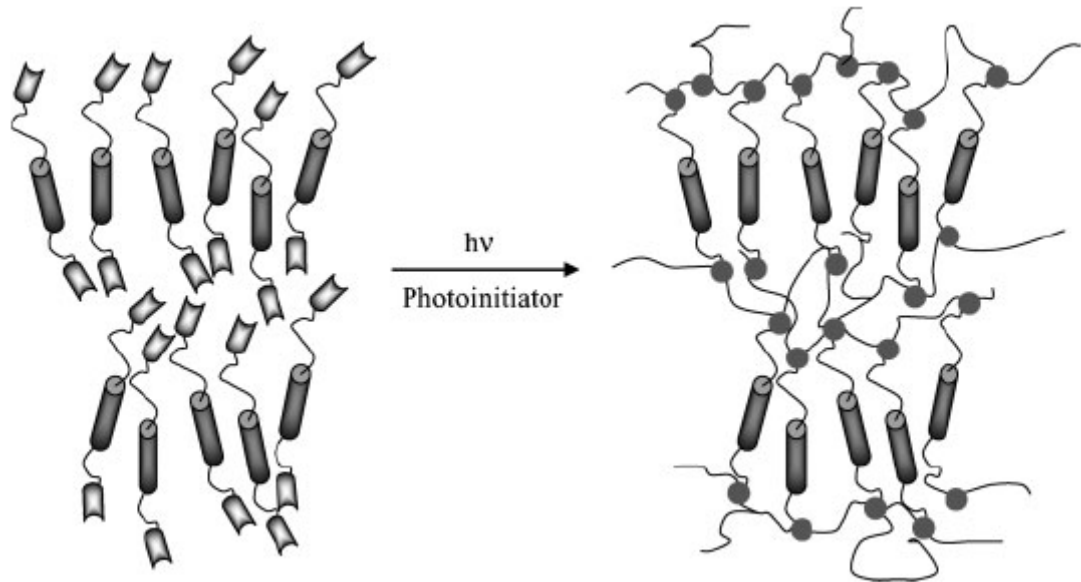
Fig.2.1 Photopolymerization of reactive mesogens.

2.2 Flow Alignment of Liquid Crystal

One of the key features in LC device is surface alignment of LC [33]. Mechanically rubbed polyimide films have been most widely used in order to align the LC molecules. A possible explanation for the alignment mechanism of LCs on the rubbed polyimide film is that polyimide molecules acquire anisotropic orientation by the stress imposed on the film surface at the rubbing process, and the anisotropic molecular force between the rubbed polyimide surface and LCs causes the surface alignment of LCs.

The rubbing process, however, produces dust and static electricity which are serious problems for the manufacturing process of LC devices. Therefore, a number of rubbing-free alignment layers with anisotropic structures of molecular orientation have been proposed. For example, irradiation of linearly polarized UV light induces an anisotropic, uniaxial orientation of UV-curable polymer molecules, and the resulting polymer film can align the LC molecules [34]. Langmuir Blodgett films are also used as the alignment layers of LCs [35].

Liquid crystalline polymers (LCPs) are highly oriented materials. A high degree of molecular orientation of LCPs is easily induced by flows. If this flow-induced molecular orientation remains until the solidification of films, we may utilize the anisotropic structure of molecular orientation for the rubbing-free process.

In a nematic liquid crystal the long axes of the rodlike molecules align, apart from small fluctuations, in a common direction. This preferred orientation, the director, depends upon several factors such as boundary conditions at the surface, externally applied fields, or shear flow. So far it has been observed that the director always aligns nearly parallel to the direction of flow in the absence of other orienting forces. Porter &

Johnson (1967) reviewed the viscometry of LCs just prior to a dramatic increase of activity in the field. It was also certain that the shear flows themselves influenced the orientation of the molecules and that the orienting influence of the flow was often in competition with that of the boundaries. Evidence of this competition was the variation of the apparent viscosity with shear rate in a capillary viscometer. Here the apparent viscosity was highest at the lowest shear rates and decreased to a limiting value as the shear rate was increased. Presumably the limiting constant viscosity at the highest shear rates corresponded to the molecular orientation, thought then to be parallel to the streamlines, which was dictated by the flow.

Capillary flow of LCs is understood for many mesophases, like nematic [36], cholesteric and smectic LCs [37]. Some numerical analysis and modeling also have been made. In our experiment, the RM material used is a nematic acrylate mixture. The flows of nematic LCs [38] is set forth to our view.

In our research, we only consider the simplest condition, free flowing nematic liquid crystals in weak capillary Poiseuille flow. The capillary force will create a gradient velocity that drives molecules to arrange in order. The forecasted model is as Fig. 2.2 illustrates.
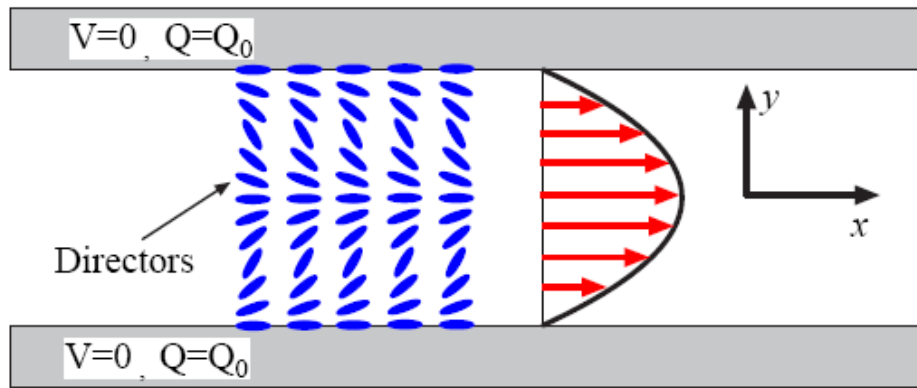
Fig. 2.2 Plane Poiseuille flow geometry. Non-slip boundary conditions for the velocity and boundary anchoring for the orientation tensor given by the stable nematic rest state are prescribed, with major director angle $\psi_0 = 0$ shown here.

The momentum transport in nematic liquid crystals shows an anisotropy as it depends on the mutual orientations of the macroscopic molecular ordering (the director n), the flow velocity (v) and the velocity gradient (grad$v$). In 1946 Miesowicz defined three principal shear viscosity coefficients of nematics [39], which can be measured in three different experiments, sketched in Fig. 2.3. In a typical experiment a magnetic field is used for molecular alignment in the nematic sample. Intuition suggests that for mesogenic elongated molecules, the lowest resistance to the nematic flow, i.e. the lowest viscosity value, should be found in the experiment presented in Fig. 2.3(b). Indeed, when the orienting magnetic field, i.e. the director n, is parallel to the velocity of the nematic flow, the lowest viscosity (η_2) is recorded. Among the two remaining viscosities, η_1 has the highest value while η_3 is close to the viscosity measured in the isotropic phase of the compound. If one excludes the temperature range in the proximity of the clearing point, the temperature dependences of the shear viscosities $\eta_1(T)$, $\eta_2(T)$ and $\eta_3(T)$ are roughly parallel to each other [40].

(a)

(b)

(c)
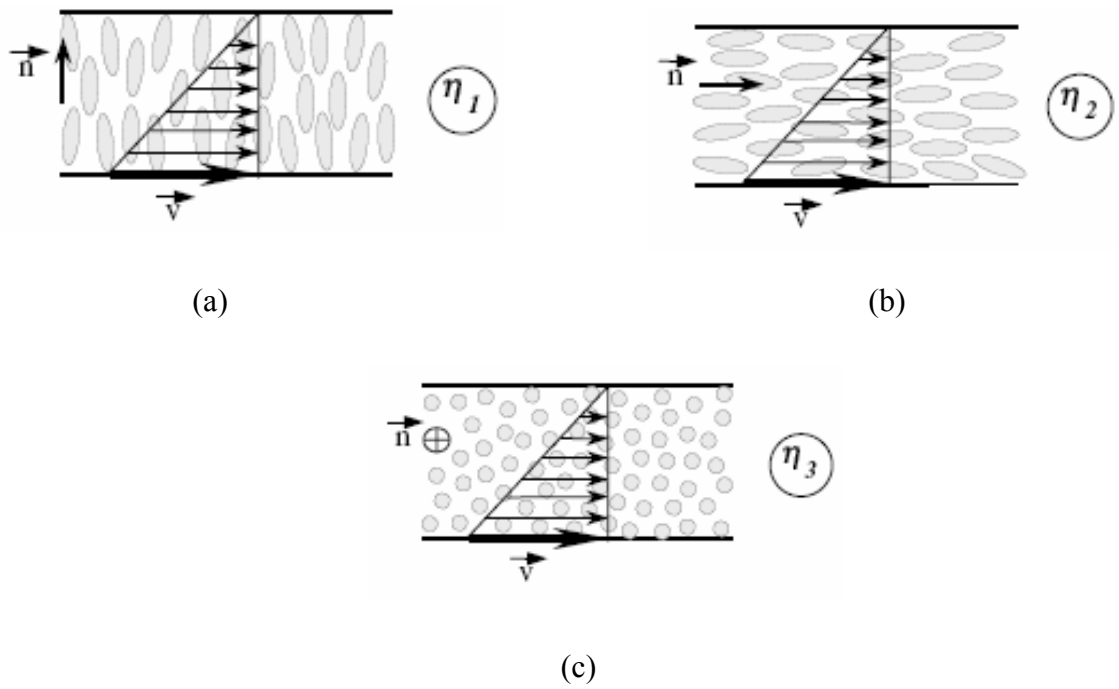
Fig. 2.3 The experimental conditions for measurements of the three Miesowicz
shear viscosity coefficients of nematic liquid crystals: (a) $n \perp v$, $n \parallel \text{grad}v$;
(b) $n \parallel v$, $n \perp \text{grad}v$; (c) $n \perp v$, $n \perp \text{grad}v$.

According to the principle of the viscosity minimum, a free fluid adopts such a
way of flow that corresponds to the minimum of its viscosity at given donditions. A free
flow of nematic liquid crystal is followed by the molecular alignment as in Fig. 2.3(b) in
the circumstances when the $\eta 2$ is the lowest possible viscosity.

Generally speaking, there are many factors, like temperature, viscosity, shear force
(induced $\text{grad}v$), molecule shape…etc, will influence the flow alignment result. The
instability of alignment flow and how to control the shear induced textural are also
widely investigated [41][42].

2.3 The Diffraction Efficiency of Gratings

Usually, we mean by diffraction efficiency (designated as DE_{+1}, or η_{+1}) the ratio of the intensities of the desired diffracted beam and the illuminating beam, measured when both beams are large enough to overfill the area of the detector being used. We ignore any power losses due to reflections at the surfaces of the grating or hologram; practical DE measurements also take these surface reflections (approximately 4%/surface, for uncoated glass) into account. This simple mathematical models overlook polarization effects, large-diffraction-angle effects, and many other subtleties of rigorous electromagnetic theory, but their conclusions can generally be extended into those domains by more detailed math, so these results serve as useful guides nonetheless.

Transmission Patterns

We describe a grating by its two-dimensional transmittance pattern. By transmittance we mean the ratio of the electrical wave fields just after and just before the grating at the same x,y location. In the simplest case, the wave is simply attenuated, so that its electric field amplitude diminishes. This is called an amplitude transmittance grating.

$$t_{amp}(x, y) = E_{out}(x, y)/E_{in}(x, y) \qquad (2.1)$$

Sinusoidal Transmittance Grating:

Here, the amplitude-only transmittance is a perfectly-smoothly-varying sinusoidal function of position, an ideal simplest case. Such a pattern could be produced by a low-contrast interference pattern exposure, for example. The most striking geometrical property of diffraction by such a grating is that there are only two output beams, the $m= +1$ and $m= -1$ orders, on either side of the straight-through $m= 0$ beam. In the far-field

pattern, we see only one spot of light on each side of the zero-order beam for each sinusoidal component of the grating's amplitude transmittance; it acts as a kind of Fourier transformer! This property can readily be proven by matching the amplitudes and phases of sets of waves on both sides of the grating (boundary condition matching). The intensity of each of the $m = \pm 1$ beams varies as the square of the amount of swing of the sinusoidal modulation, and is given by the formula to the right. Because the transmittance has to stay between zero and one, the maximum value of Δt is 0.5 (only possible if $t_0 = 0.5$ also), and the maximum value of the diffraction efficiency is then 6.25%. Four times that amount emerges in the straight-through beam, and the rest is absorbed in the grating, gently warming it. This low maximum DE is not very encouraging for the brightness of display holograms! Unbleached holograms can be bright enough to be impressive under controlled lighting conditions, but it is usually quite difficult to consistently produce the maximum possible diffraction efficiency.


$$t(x) = t_0 + \Delta t \, \sin(2\pi x/d)$$
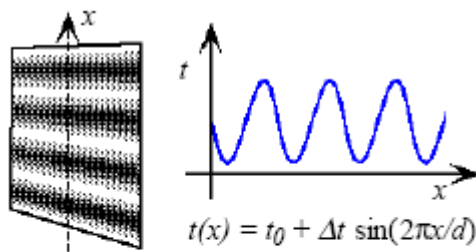
$$DE_{m=0} = t_0^2$$

$$DE_{m=\pm 1} = \left(\frac{\Delta t}{2}\right)^2 = 6.25\%_{max}$$

$$DE_{|m|>1} = 0$$

Square-Wave Transmittance Grating

Often, there are non-linearities in the exposure response of photographic materials that distort the purely sinusoidal nature of a transmittance pattern, in much the way that "fuzz boxes" can distort electrical guitar sounds. An extreme is a "hard-clipped" sine wave, which we will refer to here as a square wave or "squared-up sine wave" (that is, it is "high" 50% of the time, and "low" the other 50%) denoted as sq-sinθ. Such a grating can be considered as a summation of many ideal sinusoidal gratings, one with the same period as the square wave, and then gratings with integer fractions of that period. Each sinusoid diffracts two beams of light, so that many points of light now appear in a straight line alongside the straight-through beam. But in spite of the energy going into the extra beams, the first- order beams are brighter than before! This is because the "fundamental sinusoidal component" of a square wave has a magnitude that is larger than the magnitude of the square wave itself by a factor of $4/\pi$. So, we get transmittance values greater than unity and less than zero for that particular grating component, a physical paradox. The application of Fourier theory produces these predictions of the diffraction efficiency: more light in the first order image, by 62% (when $\Delta t = 0.5$) giving over ten percent diffraction efficiency, plus some higher orders. Note that there are no *even* orders though; this depends on the grating being exactly 50/50 open/closed.
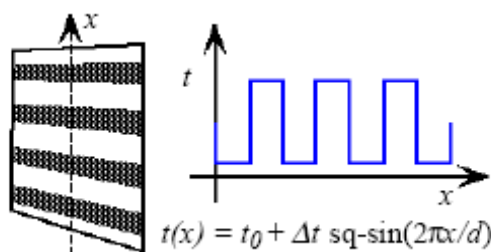
$$DE_{m=0} = t_0^2$$

$$DE_{m=\pm 1} = \left(\frac{2\Delta t}{\pi}\right)^2 = 10.1\%_{max}$$

$$DE_{m=even} = 0$$

$$DE_{m=odd} = \frac{1}{m^2} DE_{+1}$$

$$\sum_{m \neq 0} DE_m = \Delta t^2 = 24\%_{max}$$

$$t(x) = t_0 + \Delta t \ sq\text{-}sin(2\pi x/d)$$

Square-Wave Phase Grating

One reason for dwelling on the square-wave grating is that it offers a good introduction to simple p hase-only gratings. Such gratings work by retarding the wavefronts as a function of position, and the results are hard to analyze for most modulation shapes. But if the grating comprises only two phase levels, such as 0 and p, the results follow from the same analysis used for square-wave amplitude-only gratings. Phase-only gratings absorb no light energy, so that the total amount of diffracted light can reach 100% when summed over all the orders. The modulation possible for the fundamental transmittance component becomes twice what it was in the amplitude-only transmission case, ranging from +1 to -1 in effect (when $\Delta\Phi = \pi/2$), so that the maximum diffraction efficiency can quadruple to over forty percent!

$$\phi(x) = \phi_0 + \Delta\phi \, \text{sq-}\sin(2\pi x/d)$$
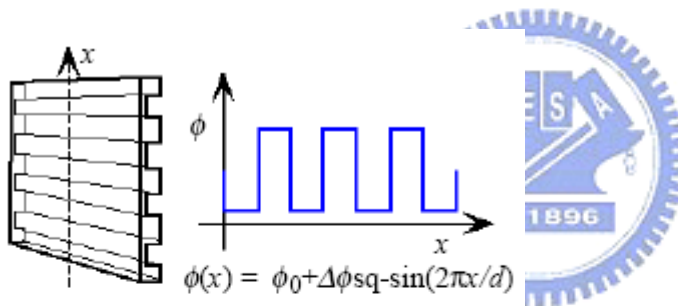
$$DE_{m=0} = \cos^2 \Delta\phi$$

$$DE_{m=\pm1} = \left(\frac{2}{\pi}\sin\Delta\phi\right)^2 = 40.5\%_{max}$$

$$DE_{m=even} = 0$$

$$DE_{m=odd} = \frac{1}{m^2} DE_{+1}$$

$$\sum_{m\neq0} DE_m = \sin^2\Delta\phi = 100\%_{max}$$

Sine-Wave Phase Grating

The depth of the phase-retarding structure varies smoothly, exactly as a sinusoid (the refractive index might vary sinusoidally instead, which is more common in bleached holograms). This turns out to be one of the few cases where the diffraction efficiency can be calculated analytically without much trouble, even though the link between phase and complex transmittance becomes highly nonlinear for only moderate modulations. For small phase modulations, the results should resemble those for sinusoidal amplitude gratings, although the phases of the first-order diffracted waves are different by 90° from the unbleached case.

The diffraction efficiencies are expressed in terms of zero- and first-order Bessel functions of the first kind, which are a lot like cosine and sine functions except that they damp down for large $\Delta\Phi$, are not strictly periodic, and the maxima of J_1 do not lie at the minima of J_0. Nevertheless, the general behavior is as expected: as the modulation increases the zero-order beam weakens and the first-order beams strengthen to a maximum DE of 33.8% (when $\Delta\Phi = 0.59\,\pi$).

$$\phi(x) = \phi_0 + \Delta\phi \sin(2\pi x/d)$$
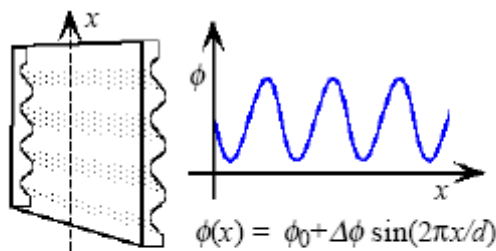
$$DE_{m=0} = J_0^2(\Delta\phi)$$
$$DE_{m=\pm 1} = J_1^2(\Delta\phi) = 33.8\%_{\text{max}}$$
$$\sum_{m\neq 0} DE_m = 1 - J_0^2(\Delta\phi) = 100\%_{\text{max}}$$

2.4 Liquid Crystal Phase Gratings (LCPGs)

Binary optical elements (BOEs) play an important role in many optical technologies because of their compactness as well as their high potential for various modifications of light phase and/or polarization. The LCs are very useful for constructing a variety of gratings since the LC director modulation can be electrically and geometrically controlled in a simple way.

A type of liquid crystal device was developed by applying a concept of liquid crystal phase gratings.   LCPGs are composed of square-wave phase gratings constructed with poly and liquid crystals which fill the grating grooves. The typical sizes of the phase grating are 1μm in width and 2μm in depth. The transmitted light wavelength can be easily controlled with changing applied voltage.

Fig. 2.4 shows a structure of a LCPG device. The light which passed through LCPG is diffracted. In a case of a plane wave of light which travels perpendicularly to the substrate, difference in refractive index between liquid crystal in grooves and grating material produce the phase shift during passing of light beam through LCPG. The two light beams interfere to each other, then specific wavelength light beams can pass LCPG as the zeroth order diffracted light.

Fig. 2.5 shows a phase diffraction grating with rectangular grooves. In Fig. 2.5, w and d represent grating constant, grating groove width and grating groove depth, respectively. In our experiments, b values are nearly twice w value. When b value is sufficiently larger than incident light wavelength, simple scalar wave theory based on the Kirchhoff's assuinption [43] can be applicable to transmittance T(λ) for the zeroth order diffraction term. The T(λ) value depends on the grating depth d and the light wavelength λ in the air, as

$$T(\lambda) = \left| \frac{1}{b} \int_0^b \exp 2\pi i [s(x)|n_{LC} - n_g|/\lambda] dx \right|^2,$$ (2.2)

where n_{LC} is the refractive index for liquid crystal and n_g is the refractive index for grating material. s(x) is grating depth over one grating period. In the case of the square-wave gratings used in the reported experiments, the s(x) value has a simple form as

$$s(x) = 0, 0 \le x \le \frac{b}{2}$$
$$s(x) = d, \frac{b}{2} \le x \le b$$ (2.3)

Introducing Eq. (2.3) into Eq. (2.2),

$$T(\lambda) = \cos^2\left(\pi d |n_{LC} - n_g|/\lambda\right)$$ (2.4)

is obtained. As shown in Eq. (2.4), T(λ) takes maximum values, when

$$d|n_{LC} - n_g| = N \cdot \lambda,$$ (2.5)

where N is zero or a natural number. Similarly, T(λ) takes minimum values when

$$d|n_{LC} - n_g| = \left(N + \frac{1}{2}\right)\lambda.$$ (2.6)

By either preparing different d value grooves or changing the LC value with varying an applied voltage, T(λ) value can be changed. Thus, the LCPG functions as an optical switch or a color filter.

For the ideal binary grating, the diffraction efficiency of the k-th order is given by

$$\eta_k = \begin{cases} \cos^2\left(\dfrac{\Delta\phi}{2}\right) & k = 0 \\ \left(\dfrac{2}{\pi k}\right)^2 \sin^2\left(\dfrac{\pi k}{2}\right) \sin^2\left(\dfrac{\Delta\phi}{2}\right) & k \ne 0 \end{cases},$$ (2.7)

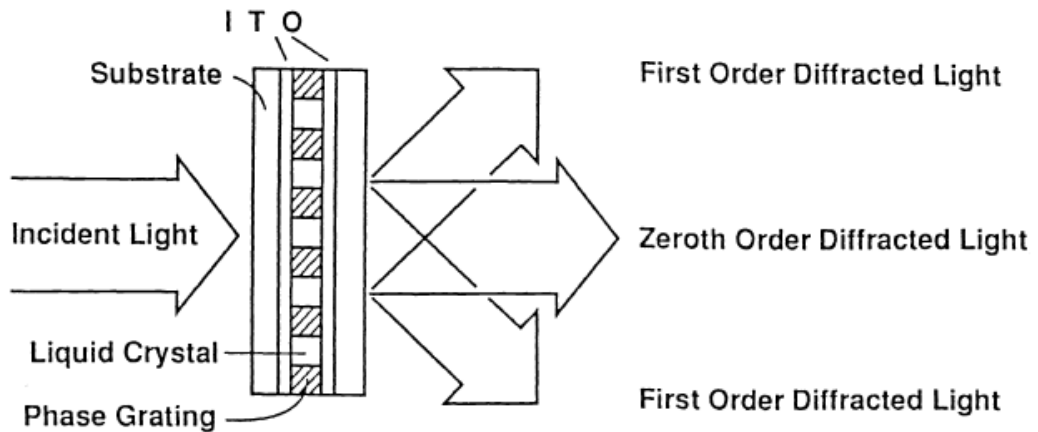where $\Delta\Phi$ is the relative phase difference between two adjacent domains in the binary grating system.

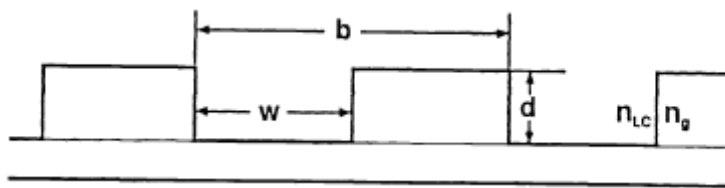Fig. 2.4 Structure of a liquid crystal phase grating.

Fig. 2.5 A phase grating with rectangular grooves. Grating parameters: b = grating constant, w = groove width, d = grating depth, n_{LC} = a refractive index of a liquid crystal, n_g a refractive index of a grating material.

For our experiment, there are some differences from common LCPG. The RM was used to establish molecular aligned phase grating structure by flowing alignment phenomenon rather than traditional alignment layer. We may take the ideal model into consideration. As Fig. 2.6 shows, when we decompose the incident light into x-direction and y-direction polarization, the $\Delta\Phi = 2\pi\Delta nd/\lambda$ is different. For y component, the refractive index difference $\Delta n = |n_{re} - n_o|$. But for x component, $\Delta n = |n_{ro} - n_o|$.
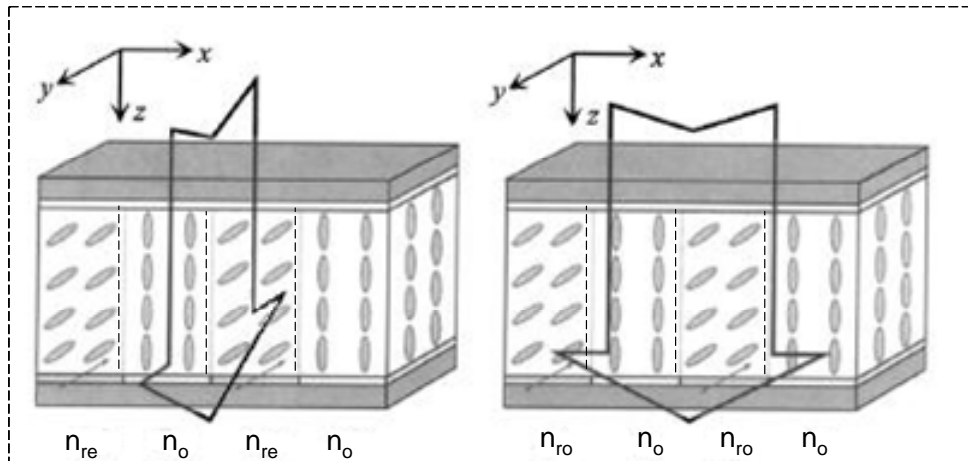
Fig. 2.6 Schematic diagram of an LCPG structure with binary phase gratings in an RM polymer grating (molecule aligned in y direction) and LC (aligned in z direction) geometry when applying voltage: (a) An input beam polarized along the *y* direction and (b) an input beam polarized along the *x* direction. The extraordinary (and ordinary) refractive indices of RM and LC are denoted by n_{re} (n_{ro}), and n_e (n_o), respectively.
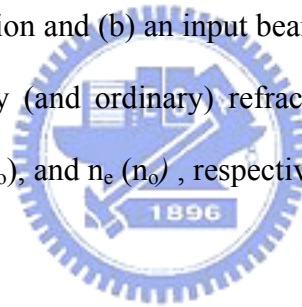
2.5 Summary

Surface-relief phase gratings were found to be useful for storing pictorial information. The information stored in gratings can be read out using projection techniques. Among this kind of devices, the phase gratings with rectangular grooves are particularly important from the standpoint of a color display device for a color image recorder. A particular wavelength light can transmit through LCPG as the zeroth order diffracted light, but the others bend as higher order diffracted lights. These phase gratings, however, have been used only as fixed image recorders. A tunable diffractive filter also has been proposed. It can regulate the change of transmitting light wavelength by varying an applied voltage. This color filter was composed of a phase grating layer and a liquid crystal layer, which are between two substrates. LCPG seems to be potentially useful for projection display devices and optical switching devices.
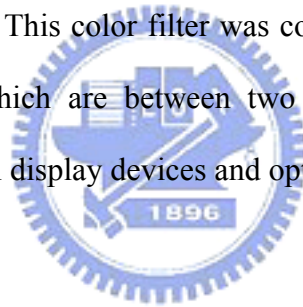
Chapter 3

Fabrication and Measurement Instruments

3.1 Introduction

A novel method to fabricate molecular aligned polymer grating in DOE was proposed in this thesis. The fabrication process will be described in this chapter.

The fabrication sequences of the proposed method included the process of the substrate and the cell formulation. The commercial available indium-tin oxide (ITO) glass was cleaned by standard process in advance. After that, the semiconductor process including spin coating of photoresist and lithography processes were utilized in order to obtain the desired grating pattern. The photoresist pattern upon the glass was taken for the micro groove that inducing the reactive mesogen flowing. Then filled with mesogen at nematic phase will be used to get the molecular orientation follow with the groove direction. After that, exposing the substrate to UV light makes photo-polymerization take effect. Finally, photoresist structure will be striped off by dipping in acetone and only polymer grating left with molecular orientational order.

The cell process joins the ITO substrates with polymer grating and another clean ITO glass. The cell gap was controlled about 2~4 μm by spacers and the space between the two substrates is filled with nematic liquid crystal. After cell process, an electric field between upper and lower ITO electrodes was applied by the function generator to measure the electro-optic properties.

The major features of the above mentioned instruments will be illustrated in this chapter.

3.2 Proposed Model

In our experiment, the polymerisable nematic mixture RMM438 (Merck) was used. The mixture is designed to give planar alignment when coated onto a substrate with suitable alignment force. The refractive indices of cured film is n_o=1.529 and n_e=1.684. The aligned polymer grating is constructed from RMM438. In order to create the alignment force for RM, the photoresist grating is formed first by lithography. We proposed a model of LC filled phase grating which can electrically tunable the diffraction intensity. The fabrication process to prepare the proposed binary phase grating is shown as Fig. 2.8.
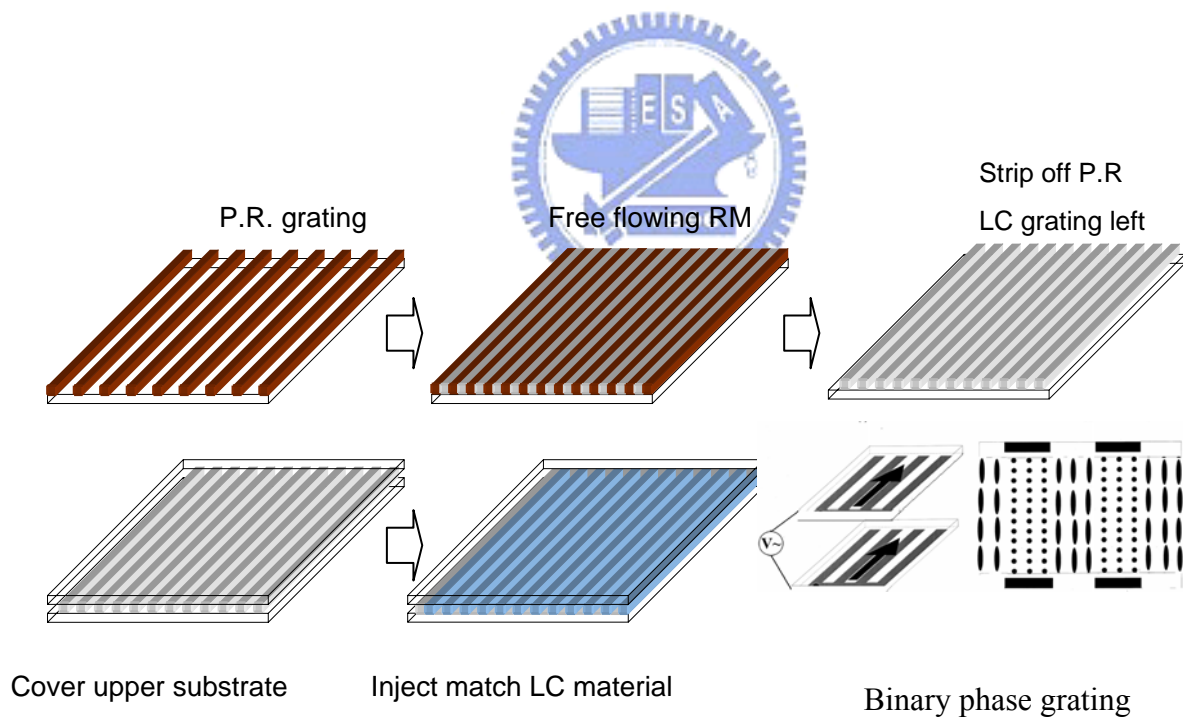

Fig. 3.1 Flowchart of fabrication process to establish our model.

3.3 Fabrication Process

The features of the novel fabrication process of molecular aligned polymer gratings have been introduced in previous section. This part will describe the cell fabrication process which includes spin coating and lithography. Moreover, the flow induced alignment process will also be explained.

3.3.1 Substrate Fabrication

The detailed fabrication steps are listed below, and the substrate pretreatment is shown schematically in Fig 3.2.

(a) Substrate pretreatment:

(1) Substrate preparation: For the Diffractive optical device, the glass is widely used as a substrate. In the fabrication, the commercial glass of about 1.1 mm thick with ITO layer was chosen. Before the lithography process, ITO glass was cleaned by detergent, acetone, isopropyl alcohol and DI water. Ultrasonic cleaning tank has been used to remove most particles.

(2) Lithography: First of all, positive photoresist FH-6400L was applied and coated on substrate. After soft baking, the ITO glass was exposed under ultra-violet (UV) light source through a mask. Consequently, the pattern on the mask was transformed to the positive photoresist after developing. Then hard baking was taken to strengthen the photoresist structure.
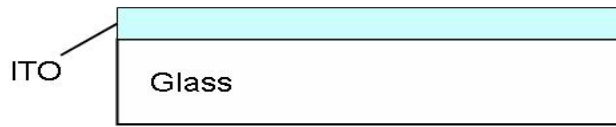
(a)
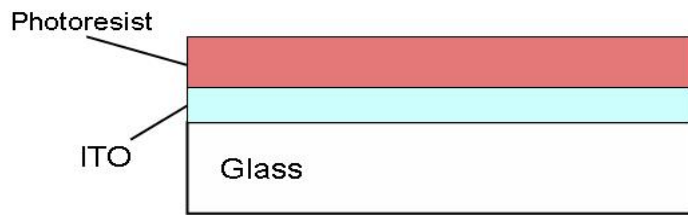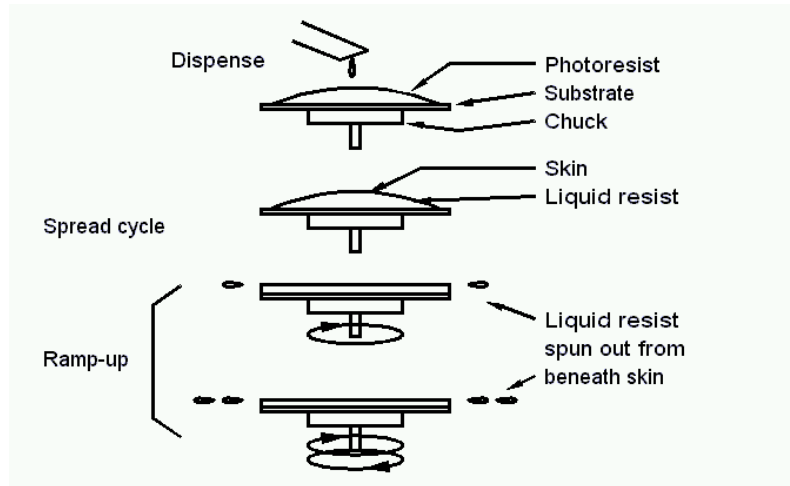
(b)
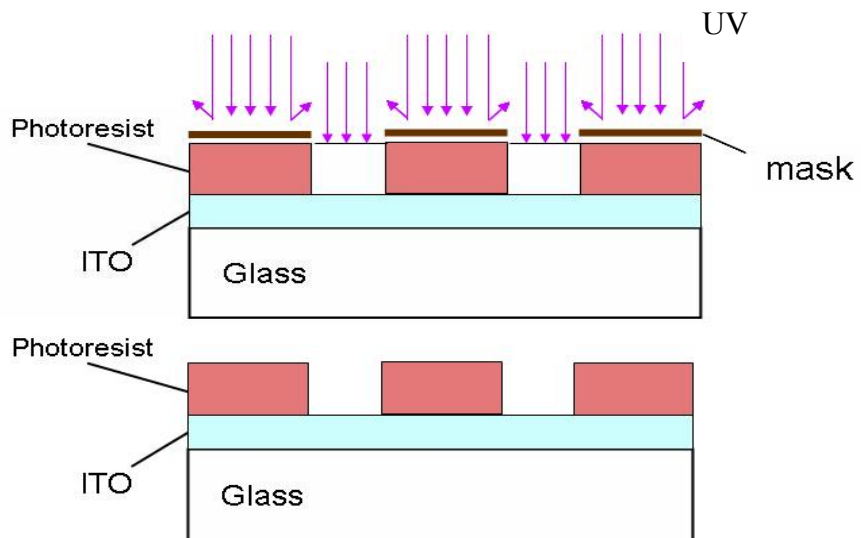
(c)

Fig. 3.2 Flow of fabricating ITO electrodes. (a) Cleaning ITO surface of the glass, (b) spin-coating Positive photoresist upon the ITO surface, (c) using lithography technique to obtain the latent image.

3.3.2 Flow Induced Alignment Process

One hot stage is needed to accurate control the temperature during flow induced alignment process. It is important to make sure the RM monomers maintain in nematic phase while flowing into pre-made photoresist gratings. After RM monomers had been pulled into the grooves by weak capillary force, UV light exposing was taken to polymerize molecules and fix the flowing aligned state. It is necessary to hold the temperature condition which can keep RM in nematic phase. After the RM polymer was fully cured the polymer gratings structure with molecular orientation were produced in desired area during UV exposing at the same time. Finally, immersing the substrate in acetone to remove photoresist and there were polymer gratings left.

3.3.3 Cell Process
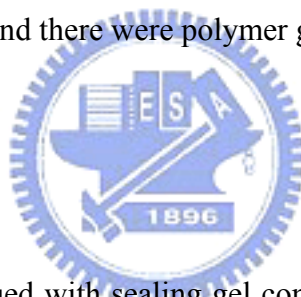
Two ITO glasses were glued with sealing gel containing spacers. The diameter of spacer with 2 μm is required for maintaining the cell gap. Finally, the space between two substrates was filled with the nematic liquid crystal.

3.4 Measurement System

After the fabrication of the polymer grating structure, the inspection will be performed to make sure that the grating structures were conformed to the expectancy. Thus, polarized optical microscope is required for observing the polymer gratings.

3.4.1 Polarized Optical Microscope (POM)

Optical microscope with the combination of an ocular and an object lens is the most popular instrument of observing a structure. A transmissive or reflective light can be chosen to observe the micro structure. Besides, a computer-controlled display (CCD) and a computer are usually equipped with the microscope and the images of observation can be taken from the CCD. In this research, a polarized optical microscope is used to study the behavior of liquid crystal through a pair of polarizer, especially. Although the magnifying power of general optical microscope has a limitation, this simple operating system still popularizes its application.

A desired angle of the linear polarized direction can be adjusted manually. Rotatable stage between the polarizer and analyzer can offer the linear polarized light transmitting the grating at any angle in normal direction. In our experiment, a polarized optical microscope was utilized to observe the anisotropic gratings in encapsulation cells.
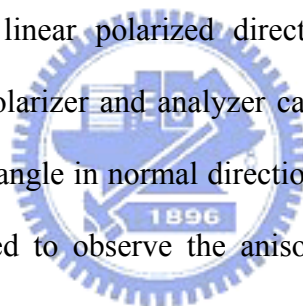
3.4.2 Atomic Force Microscope (AFM)

AFM consists of a scanning sharp tip at the end of a flexible cantilever across a sample surface while maintaining a small, constant force. The tips typically have an end radius of 2 nm to 20 nm, depending on tip type. The scanning motion is conducted by a piezoelectric tube scanner which scans the tip in a raster pattern with respect to the sample (or scans to the sample with respect to the tip). The tip-sample interaction is monitored by reflecting a laser off the back of the cantilever into a split photodiode detector. By detecting the difference in the photodetector output voltages, changes in

the cantilever deflection or oscillation amplitude are determined. A schematic diagram of this mechanism is depicted in Fig. 3.3.
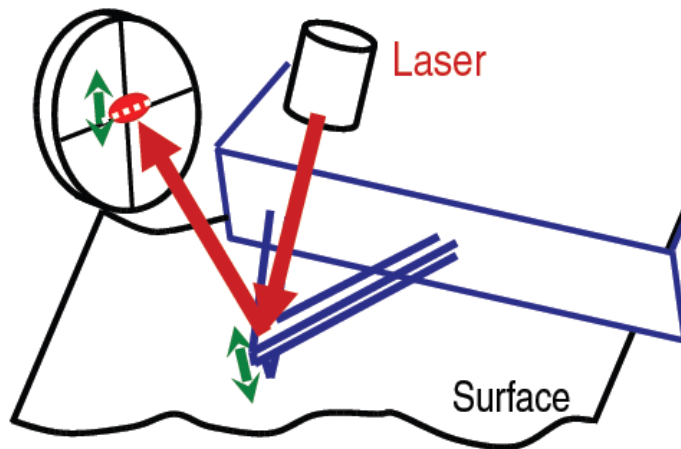

Fig. 3.3 Concept of AFM and the optical lever.

The two most commonly used modes of operation are contact mode AFM and TappingMode^{TM} AFM, which are conducted in air or liquid environments. Contact mode AFM consists of scanning the probe across a sample surface while monitoring the change in cantilever deflection with the split photodiode detector. A feedback loop maintains a constant cantilever deflection by vertically moving the scanner to maintain a constant photodetector difference signal. The distance the scanner moves vertically at each x, y data point is stored by the computer to form the topographic image of the sample surface. This feedback loop maintains a constant force during imaging, which typically ranges between 0.1 to 100 nN .

TappingMode AFM consists of oscillating the cantilever at its resonance frequency (typically $\sim 300 \, kHz$) and lightly "tapping" on the surface during scanning. The laser deflection method is used to detect the root-mean-square (RMS) amplitude of cantilever oscillation. A feedback loop maintains a constant oscillation amplitude by moving the scanner vertically at every x, y data point. Recording this movement forms the topographical image. The advantage of TappingMode over contact mode is that it

eliminates the lateral, shear forces present in contact mode, enabling TappingMode to image soft, fragile, and adhesive surfaces without damaging them, which can be a drawback of contact mode AFM. In our experiment, we make use of AFM in TappingMode to analysis surface structure.

3.4.3 Ultraviolet-Visible Spectrophotometer (UV/VIS)

The instrument used in ultraviolet-visible spectroscopy is called a UV/VIS spectrophotometer. It measures the intensity of light passing through a sample (I), and compares it to the intensity of light before it passes through the sample (I_o). The ratio I / I_o is called the transmittance, and is usually expressed as a percentage (%T). The absorbance, A, is based on the transmittance:

$$A = -\log(\%T) \tag{3.1}$$

The basic parts of a spectrophotometer are a light source (often an incandescent bulb for the visible wavelengths, or a deuterium arc lamp in the ultraviolet), a holder for the sample, a diffraction grating or monochromator to separate the different wavelengths of light, and a detector. The detector is typically a photodiode or a CCD. Photodiodes are used with monochromators, which filter the light so that only light of a single wavelength reaches the detector. Diffraction gratings are used with CCDs, which collects light of different wavelengths on different pixels.
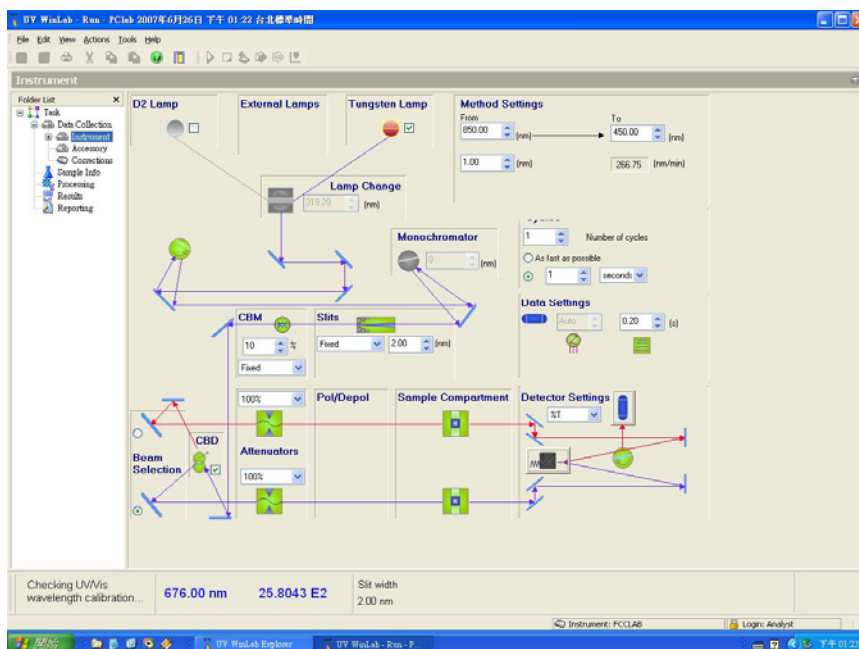
Fig. 3.4 UV/VIS spectrophotometer diagram of our set-up.

A spectrophotometer can be either single beam or double beam. In a single beam instrument, all of the light passes through the sample cell. I_o must be measured by removing the sample. This was the earliest design, but is still in common use in both teaching and industrial labs.

In a double-beam instrument, the light is split into two beams before it reaches the sample. One beam is used as the reference; the other beam passes through the sample. Some double-beam instruments have two detectors (photodiodes), and the sample and reference beam are measured at the same time. In other instruments, the two beams pass through a beam chopper, which blocks one beam at a time. The detector alternates between measuring the sample beam and the reference beam.

Samples for UV/VIS spectrophotometry are most often liquids, although the absorbance of gases and even of solids can also be measured. Samples are typically placed in a transparent cell, known as a cuvette. Cuvettes are typically rectangular in

shape, commonly with an internal width of 1 cm. (This width becomes the path length, L, in the Beer-Lambert law.) Test tubes can also be used as cuvettes in some instruments. The best cuvettes are made of high quality quartz, although glass or plastic cuvettes are common. (Glass and most plastics absorb in the UV, which limits their usefulness to visible wavelengths.)

In this thesis, UV/VIS is utilized for analysis of monomer's orientation and order parameter. Our set-up diagram is shown as Fig. 3.4.

In order to measure the variation of diffraction intensity with applied voltage. A simple laser system as established as Fig.3.5. The light source is He-Ne laser which has maximum power at 632.8 nm.
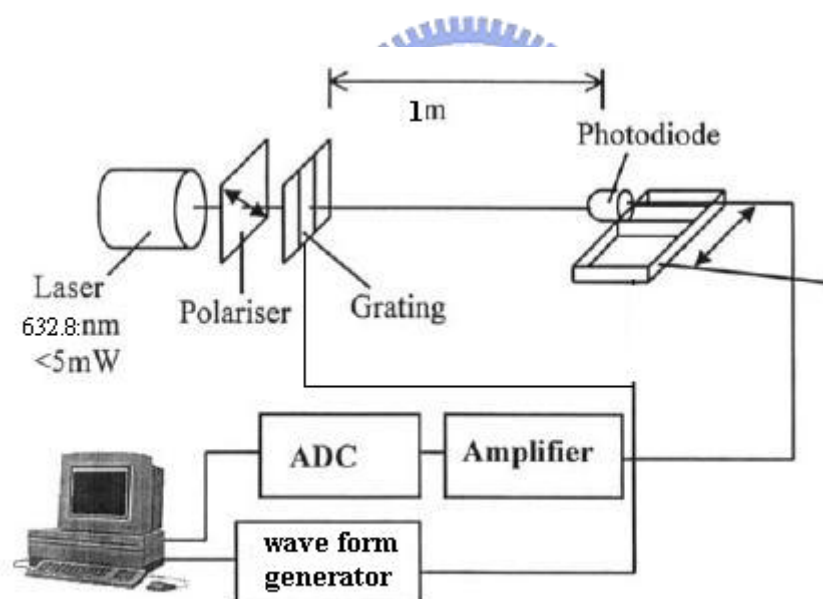

Fig. 3.5 The sketch of laser system used to measure DE.

Chapter 4

Results and Discussions

4.1 Introduction

The flow induced alignment method of polymer grating structures was introduced in previous chapter. As mentioned before, self assembly orientation neither phase separation nor fringe field effect are the main advantages of the fabrication method. This novel method can be utilized to form polymer gratings with very small periods and beautiful structures which depend on the resolution of lithography process. During operation, the LC molecules were forced to tilt following the direction of applying electric field but the RM monomer had been fixed by photopolymerization. Therefore, fringe field effect won't occur in this case. A polarized optical microscope was utilized to observe the anisotropic polymer gratings and experimental results. The surface scanning step was performed by AFM since the period of structure is too tiny to be measured by common surface profiler. Besides, the data measured by UV/VIS spectrophotometer point out the order of RM monomer's orientation. Finally, a laser system was used to determine the diffraction efficiency of DOE. All results will be shown in this chapter. After fabricating the binary phase grating, the proposed process will also be evaluated in nematic liquid crystal E7. The experimental results and comparisons will then be further discussed.

4.2 Experimental Results

Polymer grating structure in photoresist groove was fabricated by flow induced method. The first step is making sure that the flowing process is operated at correct temperature so the phase transition temperature of RM must be verified. In order to prove the figure of polymer grating was well formed and the mesogen aligned at desire direction. POM, AFM and UV/VIS spectrophotometer were used. By applying the DOE to laser system, the diffraction efficiency was acquired. The result of each subject was exhibited in different section.

4.2.1 Phase Transition of Reactive Mesogen

The temperature of polymerization was an important issue in this method, and the temperature will greatly affect the result. In order to observe the phase transition temperature of reactive mesogen, a hot stage and polarized optical microscope was required. The temperature can be exactly controlled by the hot stage. As the observation by the microscope shown, the phase transition temperature of RM is shown in Tab. 4.1 and Fig. 4.1 displays picture at each observing temperature. In order to get the smaller viscosity and higher flowbility in nematic phase , it was decided to operate the flowing process at 70℃. As the Fig. 4.1 (h) shows the RM is a nematic acrylate mixture, it appears some bright flakes while other area is at isotropic state. Therefore, the phase transition temperature will cover a region of temperature.
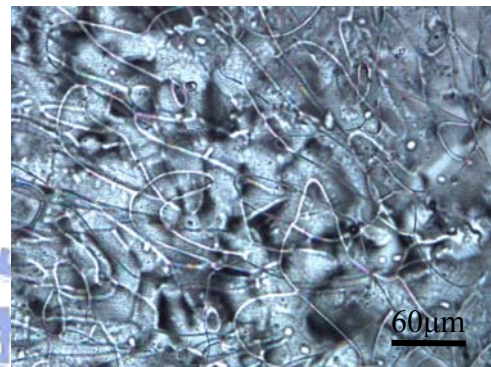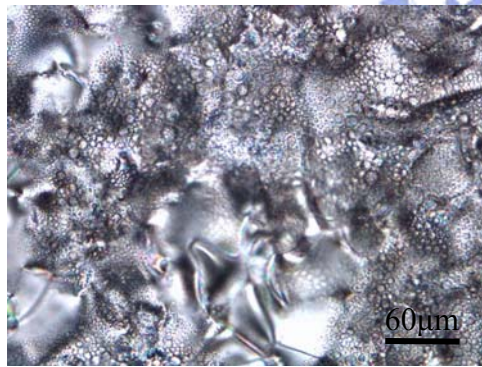
Tab. 4.1 The phase transition temperature of RM.

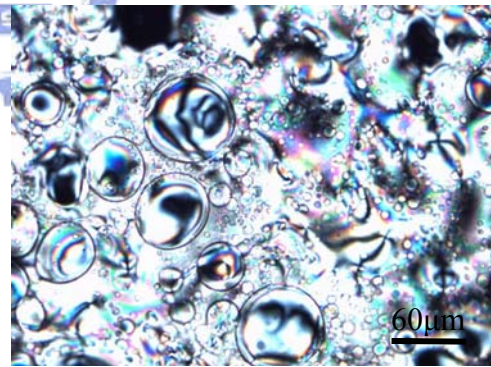| Phase	Crystal	Nematic	Isotropy
Temp.	＜35℃	40℃～72℃	＞74℃

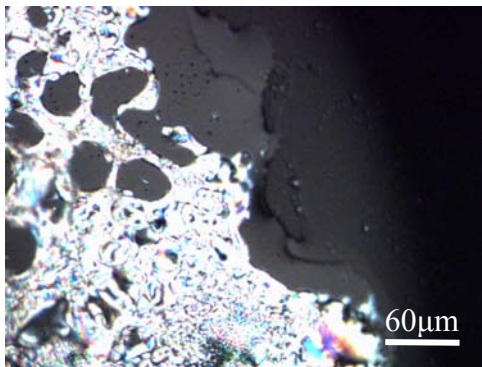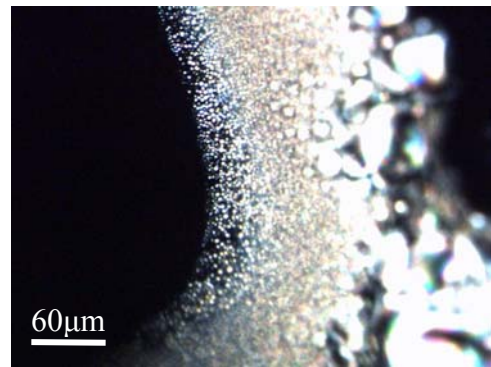(a)   (b)

(c)   (d)
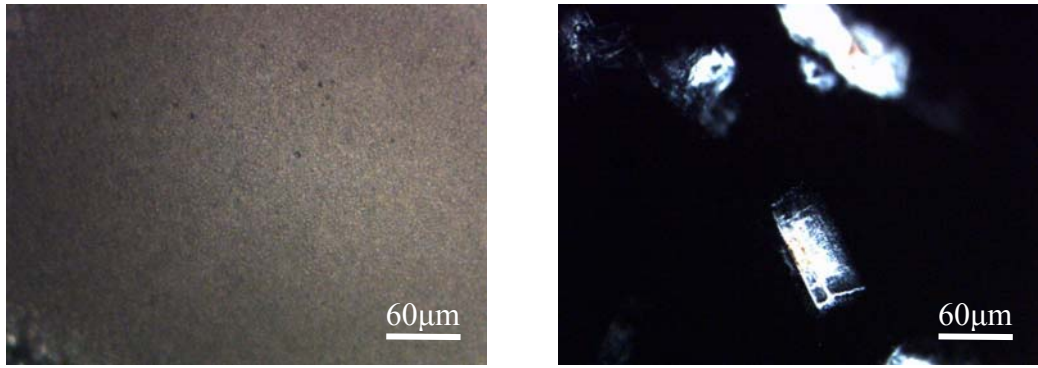
(e)   (f)

60μm

60μm
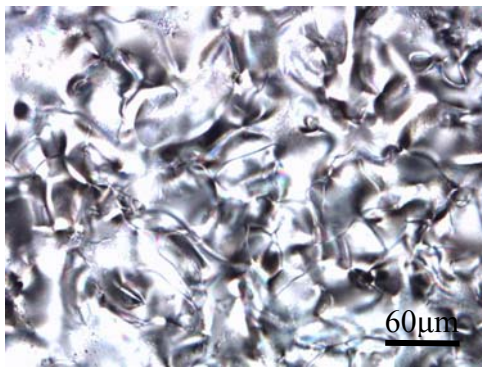
(g)   (h)

Fig. 4.1 The photographs of RM438 were taken at (a) 24.8℃ (b) 40℃ (c) 60℃ (d) 72.9℃ respectively. The images (e) 73℃ and (f) 72.6℃ show the transition states between nematic and isotropy during raising and cooling procedure. The phase of RM can be observed while cool to (g) 65.8℃ and (h) shows bright flakes while other area is at isotropic phase.

4.2.2 Photolithography Result

In order to create aligned RM grating, the photolithography technique was utilized to build micro grooves that can provide a week capillary force to induce RM molecules orient toward the direction of photoresist grooves. Consequently, The photoresist structure will influence directly on flowing result, especially The boundary between RM and photoresist. It is necessary to analysis the photoreisst structure to make sure the photolithography process is acceptable for next RM flowing step. Fig. 4.2 shows the images of photoresist surface structures that were scanned by AFM. The flow induced defect will formed with the unsmooth structure of photoresist. Thus, the beautiful photoresist structure is the first factor in forming well aligned gratings. Fig. 4.3 displays the pictures of photoresist taken by POM.
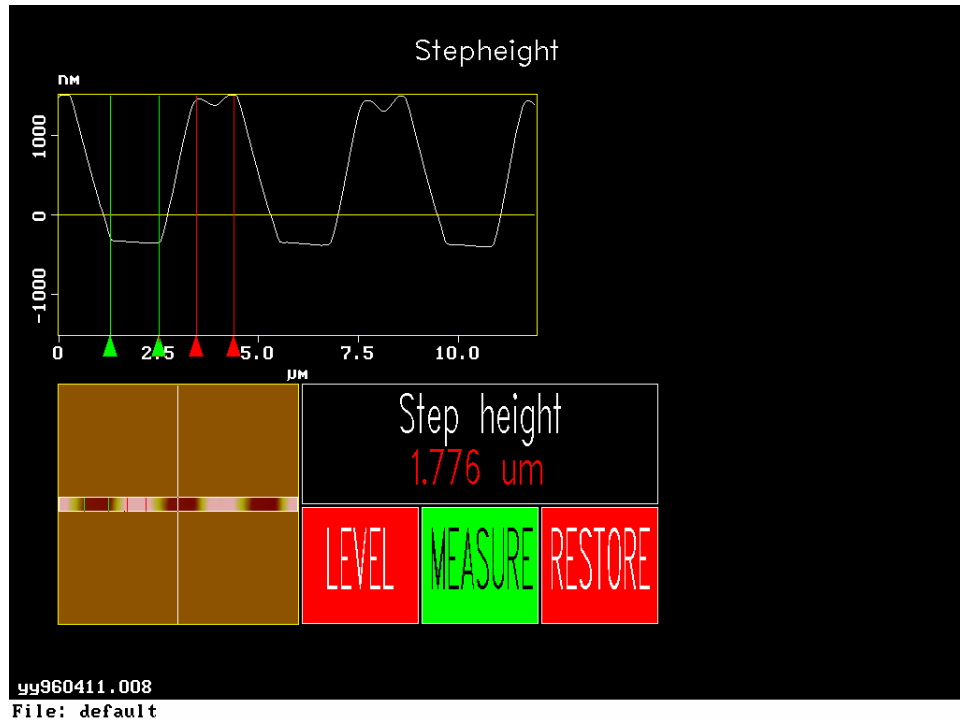
45

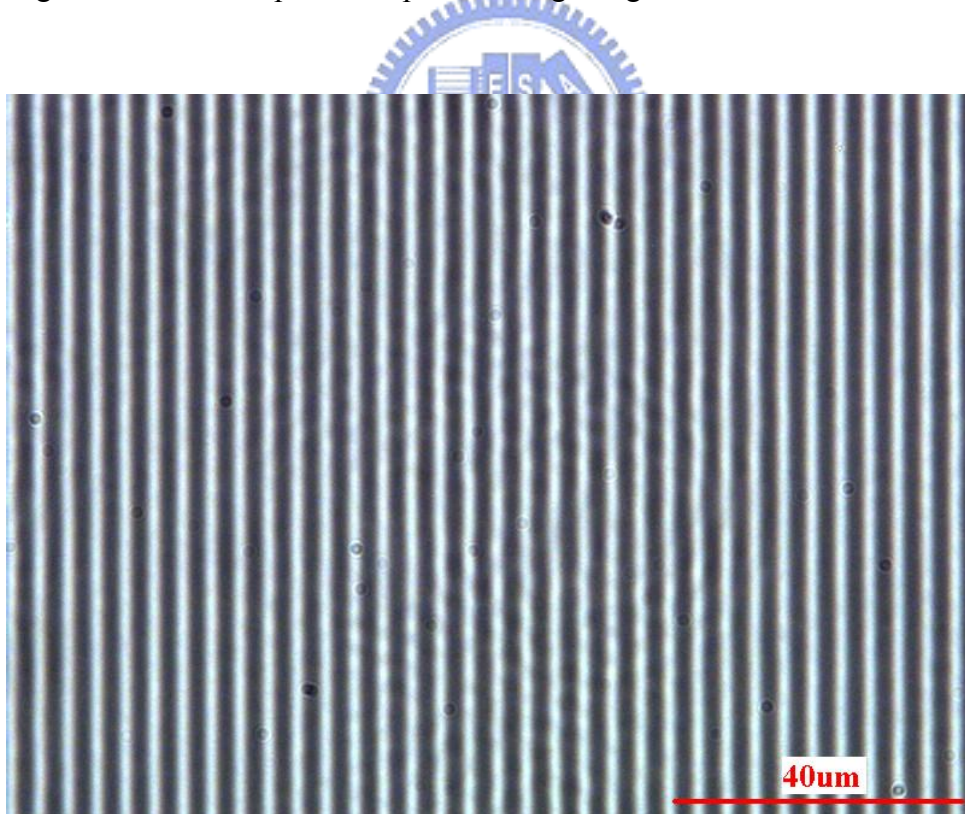Fig. 4.2 The surface profile of photoresist grating.

Fig. 4.3 The POM image of photoresist grating.

4.2.3 Flow Induced Alignment Result

After photolithography procedure, RM had been drop filled on the PR grating surface. By controlling the temperature at 70℃, RM was held on nematic phase. The PR grooves provide a weak capillary force for RM and draw molecules into grooves. Then the mesogen will oriented along the direction of flowing because of the freely flowing properties of nematic liquid crystal. The aligned state was fixed with photopolymerization of RM while exposing to UV light. In fact, the temperature of flowing, the condition of PR gratings and the capillary force it provides will greatly affect the quality of RM gratings. Fig. 4.4 shows the experimental result of the RM grating which was flowing and polymerized at different temperature.
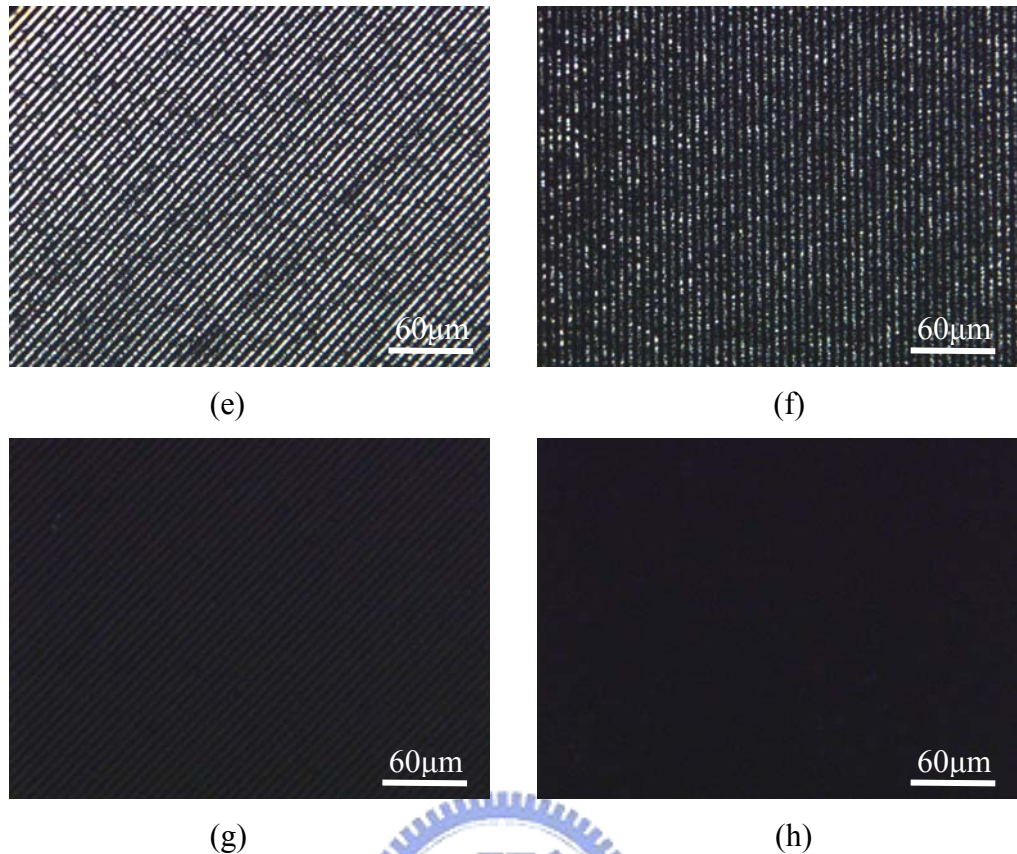

| (a) | (b) |
| (c) | (d) |

(e)

(f)

(g)

(h)
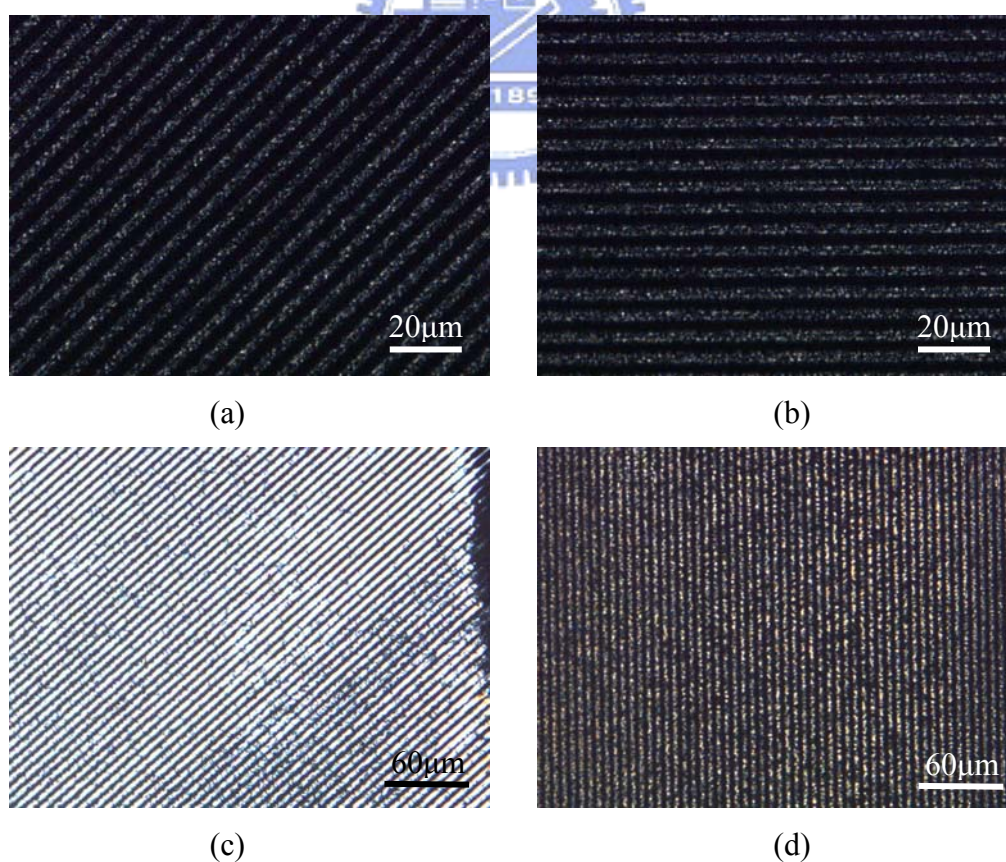
Fig. 4.4 The flowing result of polymer gratings at (a)(b) 70℃ (c)(d) 65℃ (e)(f) 60℃ (g)(h) 55℃. There is an include angle 45 degree between the crossed polarizers and the direction of RM gratings at (a) (c) (e) and (g). The others, at (b) (d) (f) and (h), the include angles are 0° or 90°.The spacing of gratings is 3μm.

The results will be affected by different flowing temperature. If the device is flowing at the temperature higher than nematic phase region, RM will lose its dichroism. Light transmission is independent of the direction angle of linear polarized light. It is to say that the image is always dark while the polymer grating rotates between the polarizer and analyzer. In other words, the linear polarized light will see different refractive index while rotating the grating with well aligned molecules in one major direction order. The higher order which the molecules aligned the higher contrast ratio we could get.

Capillary force of PR grooves is another issue we should concern. In our experiment, we only can adjust the spacing of PR groove to find the best condition. The spacing of PR grating 1μm, 2μm and 3μm are fabricated to be flowing groove. The result as Fig. 4.5 shows that 1μm spacing can induce less defect aligned polymer grating but there are too many disclination lines in 3μm spacing. Although 1μm spacing can get the best result, we still choose 2μm spacing as our major condition. Because 1μm spacing has already reached the limitation of the mask aligner we use, the yield of 1μm grooves is too low.

(a) 1μm   (b) 2μm
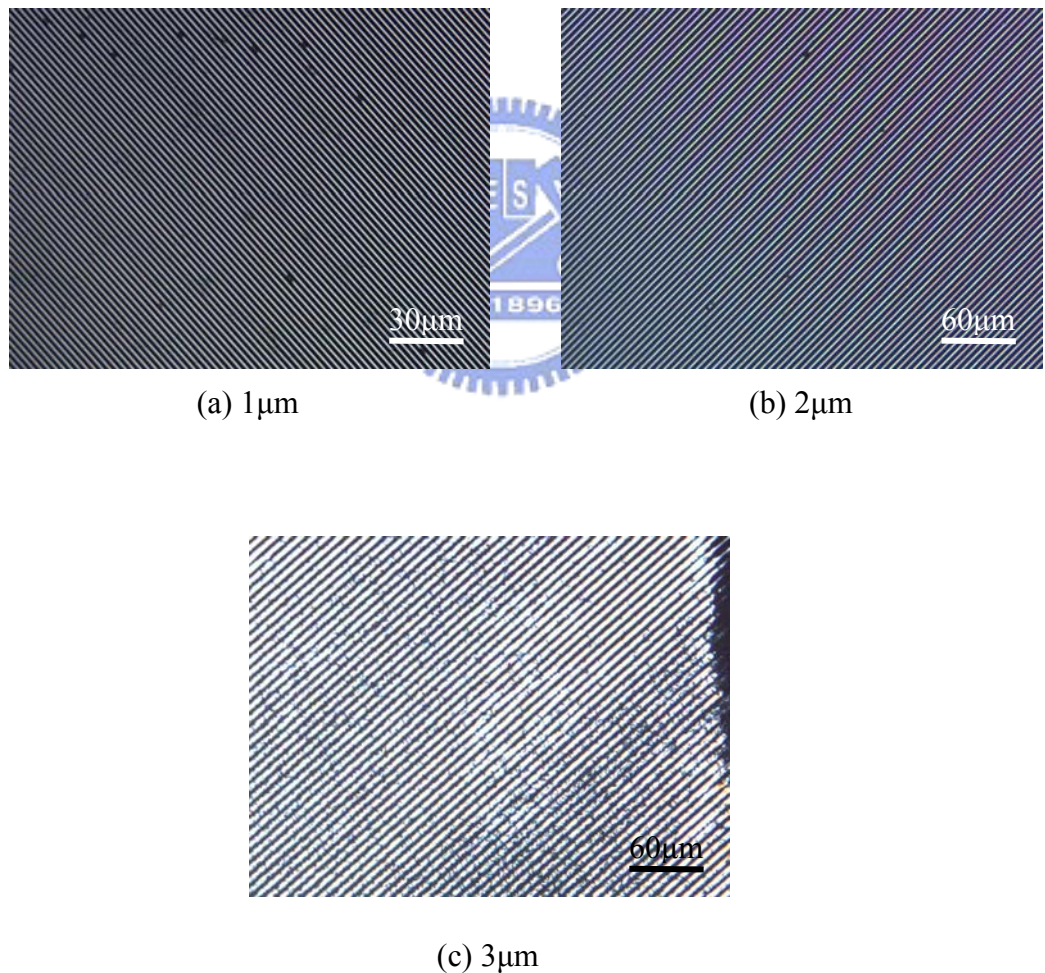

(c) 3μm

Fig. 4.5 The photographs of different spacing (a) 1μm, (b) 2μm and (c) 3μm
        polymer gratings.

The flowing process time of fabricating polymer gratings is about 20 minutes. After curing process by UV light, the remains photoresist was stripped off by acetone and leaved polymer only. Fig. 4.6 presents the structure of polymer gratings scanned by AFM. As we mentioned, the RM is free flowing into the PR grooves by weak capillary force. The structure of the polymer grating will vary with distance. We could observed that the structure of polymer gratings are still not a perfect square shape and the top surface of the grating was concave as indentation which may caused by the mutual action between the RM monomer and PR. Another reason is shrinking effect that may result in the sunken surface.
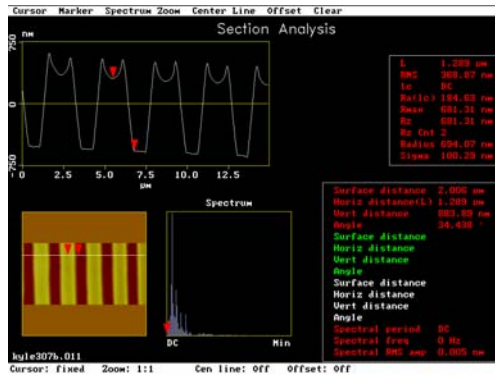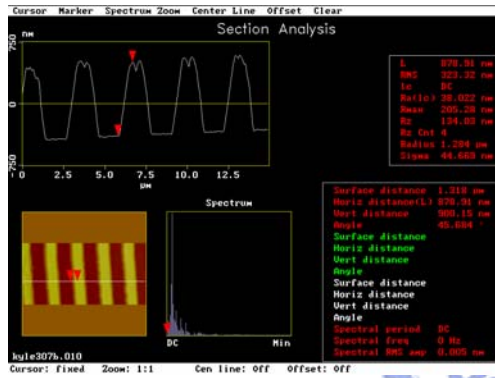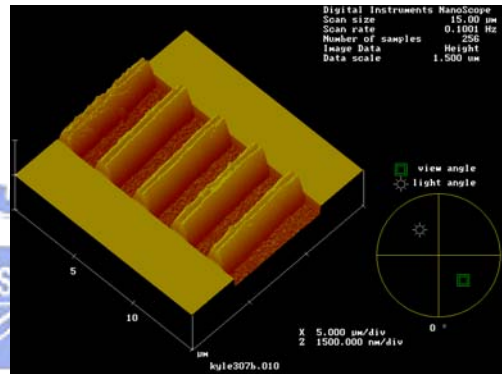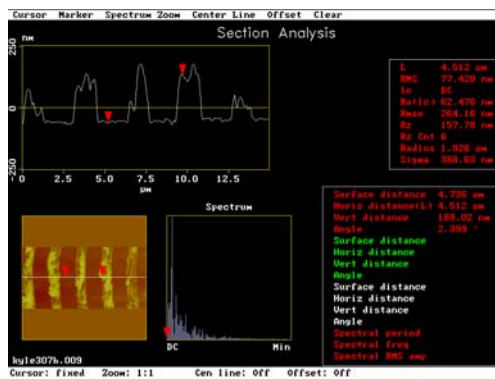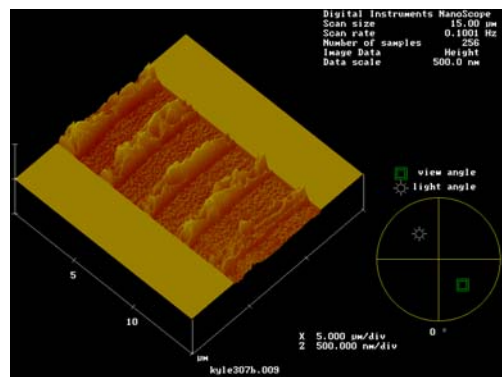
(a)
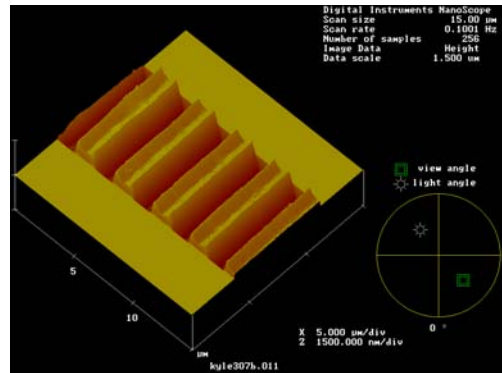
(b)

(c)

(d)

(e)

(f)

Fig. 4.6 The surface structure of RM grating (a) (c) (e) were
scanned at wave source, flat area and wave front
respectively.(b) (d) (f) are simulated 3-D structure.

51

4.2.4 The Orientation Order of Molecules in RM Grating

To quantify the orientation order of molecules, UV/VIS spectrometer is set up with crossed polarizer and analyzer. The sample was build between them and the transmittance was measured while rotating the sample. The transition curve vs. included angle between the grating direction and polarizer is shown in Fig. 4.7. As the result shows, the first maximum transmittance appears at 45 degree with a period of 90 degree. It can easily determine what direction of molecular orientation order is. It also can suggest that the orientation direction is followed with the flowing direction.

Another absorbance measurement is also carry out by UV/VIS. 1wt% dichroic dye S-428 was mixed into RM. The molecules of dye can align with RM and provide a great absorbance at wavelength 500~600nm. The order parameter of dye, S, can be determined by the absorption $A_{\parallel}$ and $A_{\perp}$ using $S=(A_{\parallel}-A_{\perp})/(A_{\parallel}+2A_{\perp})$ [44] at 500nm of the wavelength under polarized UV/vis spectrometer. The mid-order parameter, S=0.48, can be achieved by flow induced alignment in micro-grooves with 2μm spacing. Fig. 4.8 displays the difference of absorption spectrum $A_{\parallel}$ and $A_{\perp}$ of the dichroic dye.

(a)

(b)
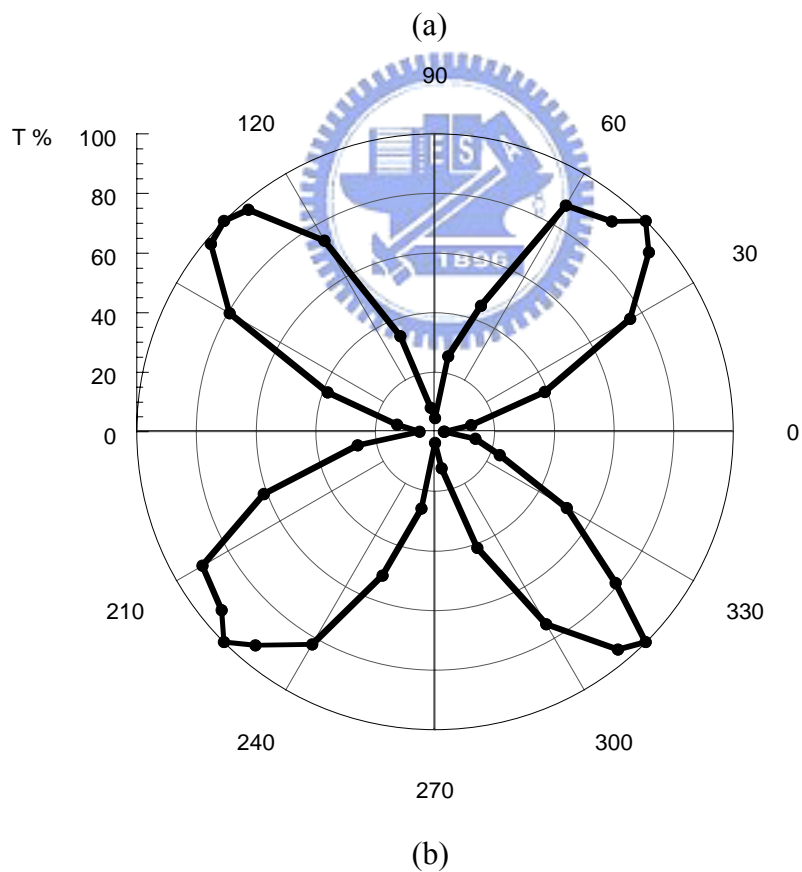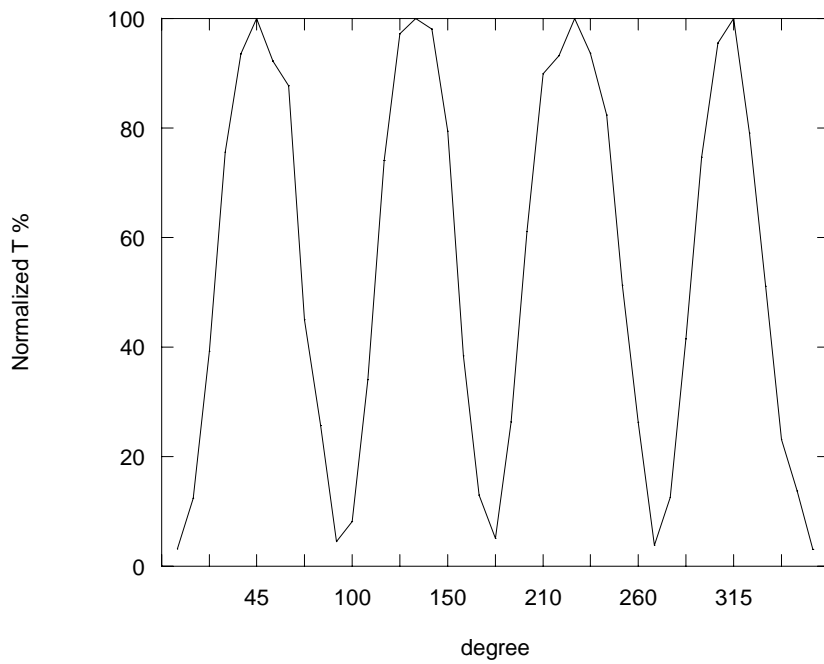
Fig. 4.7 The transmittance vs. rotation angle at 550nm in (a) Cartesian
coordinate system and (b) Polar coordinate system. The
spacing of polymer grating is 2um.
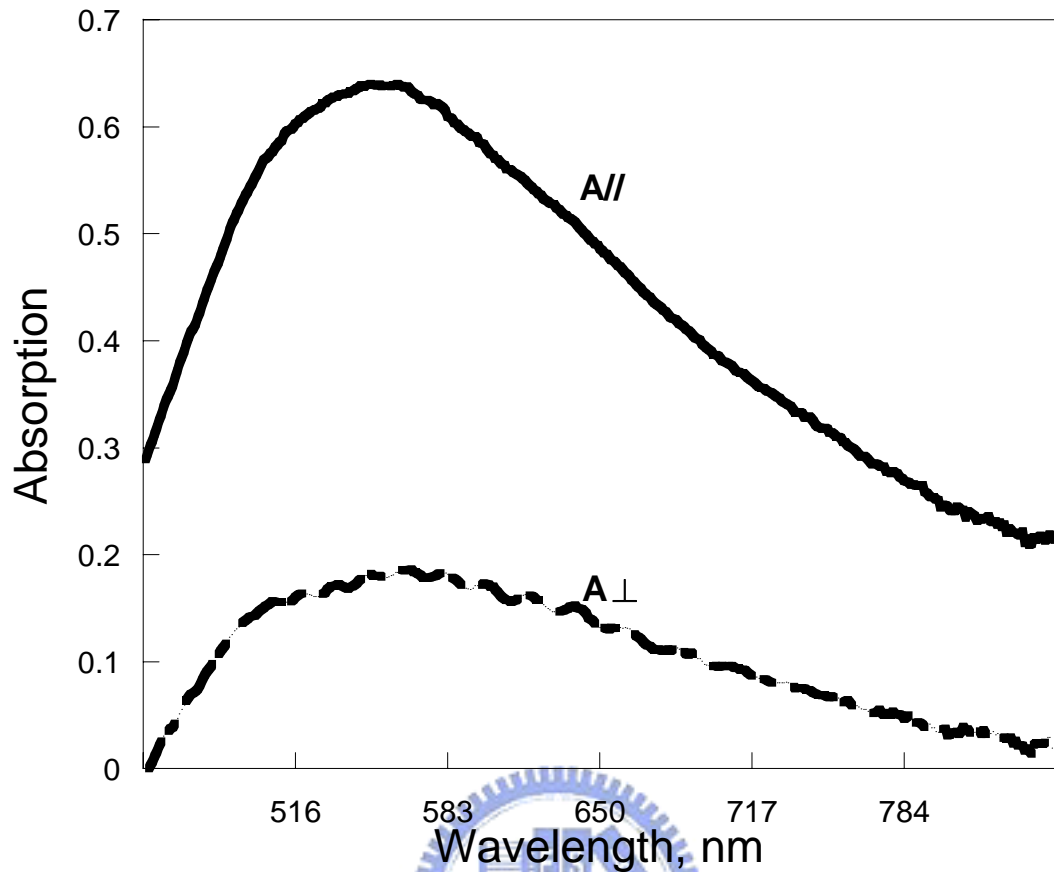
Fig. 4.8 The absorption spectrum of the dichroic dye in RM grating. $\parallel$: the direction of grating parallel to the direction of linear polarized light. $\perp$: the direction of grating perpendicular to the polarized light.

4.2.5 The Defect of Free Flowing

Although the self-aligned property can be observed by free flowing method, there are still some defects and instabilities coming up with this process. The grooves provide a weak capillary force. The inter-work between PR boundary and flowing force induce a weak gradient velocity from center to the each side. When laminar flow occurred during free flowing, the orientation director will follow the flowing direction and force

the bulk of molecules aligned. Actually, we can still observe light leakage while the orientation order of the bulk LC is parallel or perpendicular to the polarizer. It means that not all of the molecules are oriented in the same direction. Fig. 4.9 displays the aligned defect results in the light leakage. There is another phenomenon that could be observed. By the method of free flowing, some disturbance will happen in the wavefront. The effect will reduce the uniform area. The season of the disturbance is free flowing type can not apply a steady pressure from the source. Therefore, the wavefront is not the only one in the same groove but appear continuously with different period. To prevent the defect, a pressure source that can control the steady velocity of flowing is necessary. Fig. 4.10 presents the disturbance area which include a angle about 45 degree from the bulk direction of alignment.
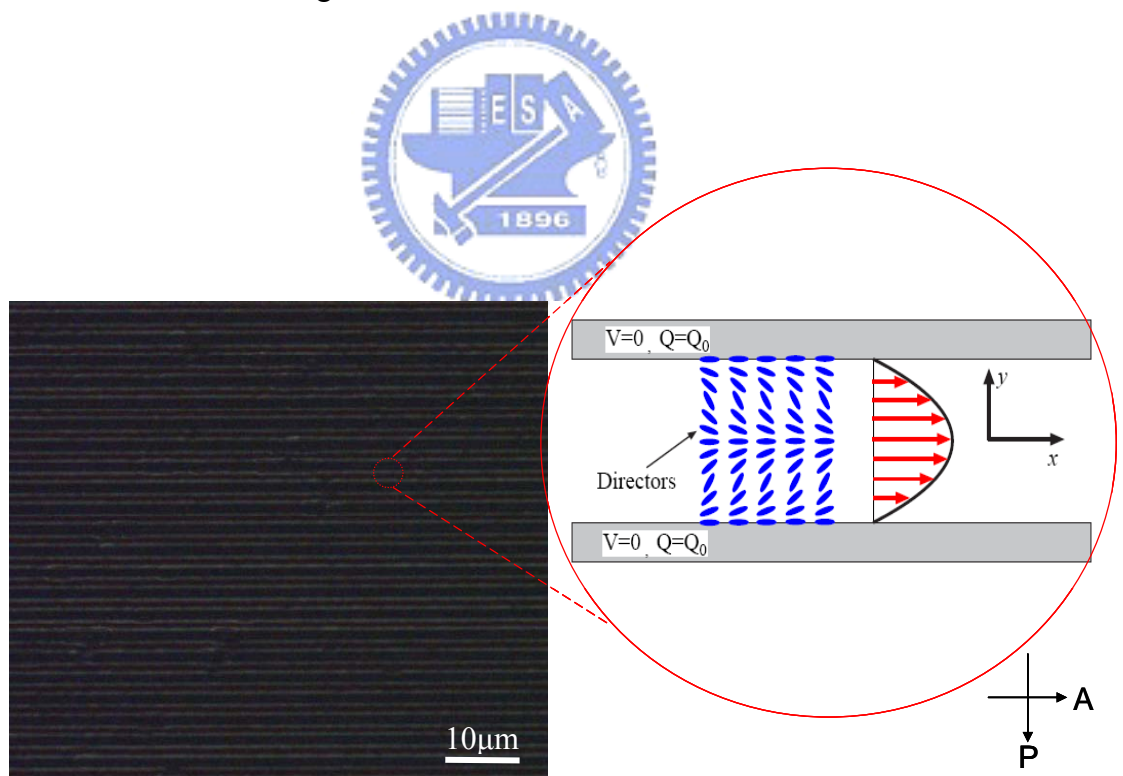
Fig. 4.9 The light leakage appeared under crossed polarizer because of the
alignment defect.
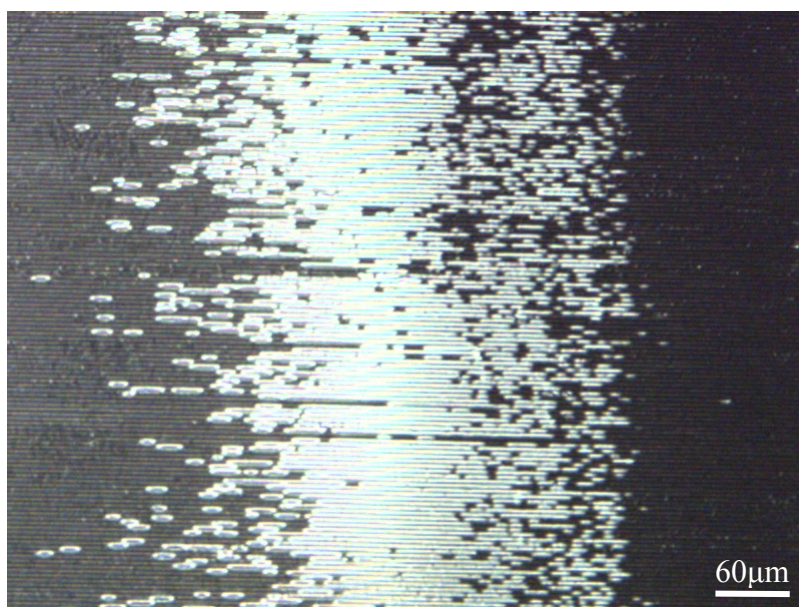
(a)
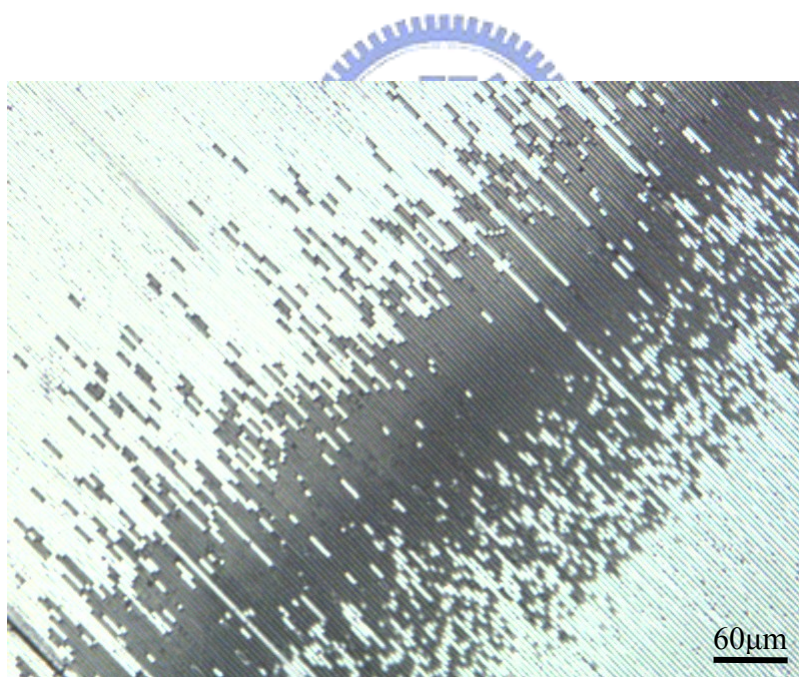
(b)

Fig. 4.10 The disturbance area shows opposite state to the bulk of grating. (a) The
bulk orientation order is parallel to the polarizer. (b) Rotating a angle
about 45degree from the direction of polarizer.

4.2.6 The Diffraction Efficiency of RM grating

After the cell process, RM grating between ITO glasses could be established. The cell was filled with nematic LC, E7 and measured the diffraction efficiency with applied voltage. The diffraction pattern is shown as Fig. 4.11. The diffraction pattern has appeared while no voltage was applied. This is because of the mismatch of refractive indices between RM and E7. The maximum DE of first order was occurred when we applied about 1 volt on the cell.

(a)

(b)   (c)
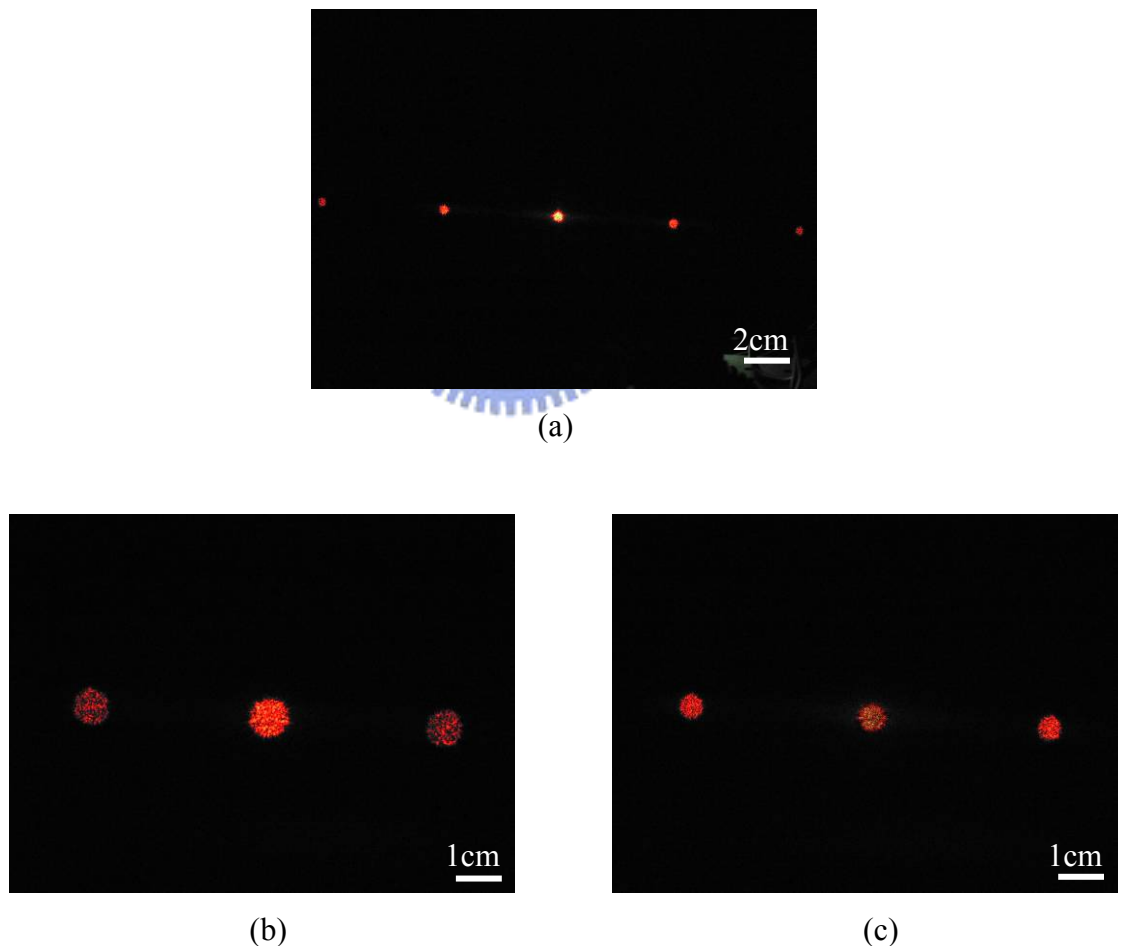
Fig. 4.11 The pictures display the diffraction pattern of LCPG including zero order, first order and second order (a). The variation of zero order and first order while applying 0 volt (b) and 1volt (c).

The tuning property of DE is recorded as Fig. 4.12. There is still a difference between the actual and ideal value. In theory, the maximum value of DE can reach 40.5% as we mentioned in chapter 2. The disagreement may result from the imperfect square wave of phase profile, the defect of alignment and the insufficient retardation of LCPG.
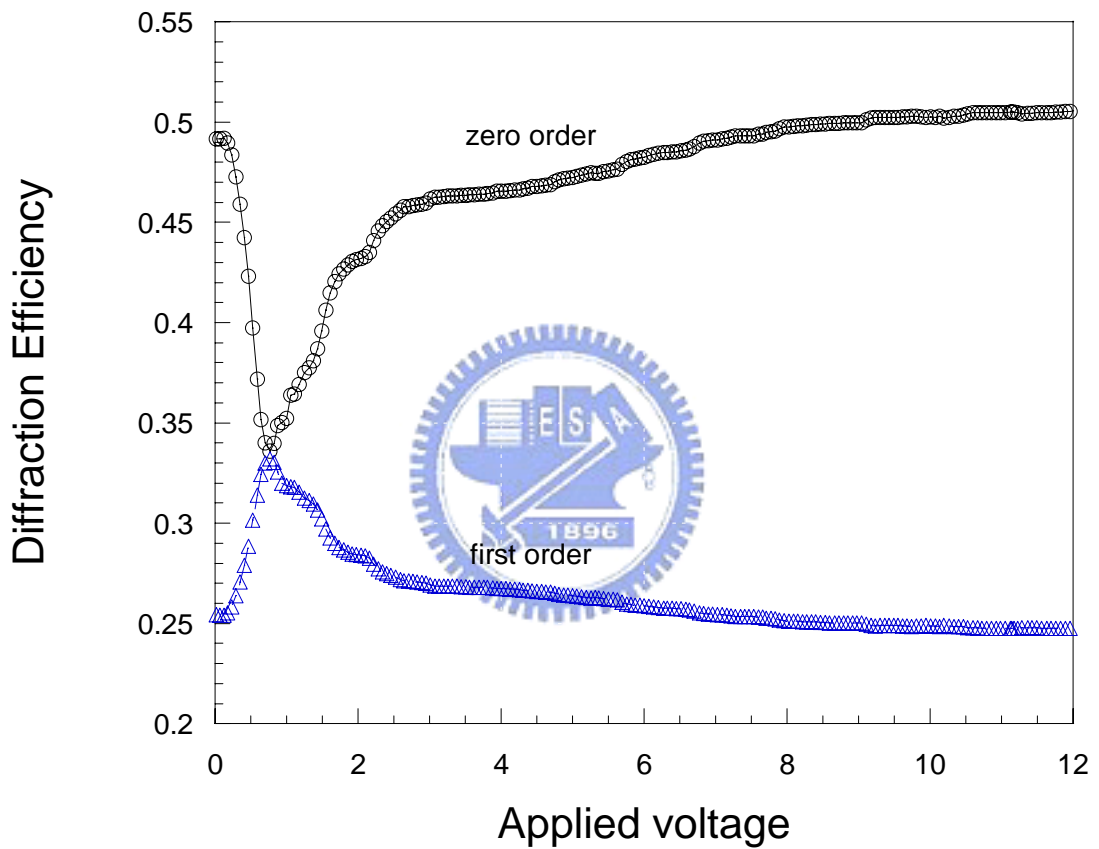
Fig. 4.12 The sketch illustrates the relationship between DE and applied voltage. The polarization direction of laser beam is parallel to the direction of gratings.

4.3 Discussion

The DOE were widely utilized in optical communication, optical storage and display applications. The popular method to fabricate tunable binary LC diffractive grating device is to use holographic polymer-dispersed LC (H-PDLC) or patterned electrode method. Nevertheless, the electric field induced phase grating method has the limited grating spacing because of fringing effect. The H-PDLC method also has the phase separation and scattering problem. All of these are the reason that will decrease diffraction efficiency. Neither incomplete phase separation nor fringing effect problem took place in the method we proposed.

Compared with H-PDLC method, phase separation between LC and reactive monomer will decide the boundary quality between LC and polymer. The smoother polymer wall the more scattering effect that can be prevented. In our experiment, the boundary between LC and polymer is decided from the lithography procedure. The edge surface of the PR grating will contact the RM directly during flowing process. To maintain a good lithography quality is contributive to decrease the aligning defect occurred in flowing method. Another advantage of our design is that the polymer molecules in the device were fixed by the photo-polymerization. The electric field will take no effect on the area polymers exist. As the result, the patterned electrodes are not needed and the fringing effect won't happen. Actually, there is another basic difference from other method. The alignment of RM was not induced by traditional alignment layer but week capillary force. Tab. 4.2 shows the comparisons of proposed and conventional processes.

Tab. 4.2 Comparisons of proposed and conventional processes.

Process	Flow Induced	H-PDLC	Patterned Electrode
Grating			No solid structure
Photo-mask	Need	Without	Need
Alignment layer	One or without	Need	Need
Advantage	No fringing effect, no phase separation, beautiful grating structure, micro or sub-micro structure could be developed	Polarization control, easy fabrication, stackable of organic polymer	Easy fabrication Low absorption
Disadvantage	Free flowing wave form distortion, free flowing instability and small effective area.	Shrinking effect, light scattering, spacing depend on PDLC quality	Fringing effect limits grating spacing.

4.4 Summary

Aligned Polymer grating structures can be successfully fabricated by flowing induced method. The free flowing temperature of RM in 2μm and 3μm spacing are 70°C and 65°C, respectively. In addition, free flowing method has some instability. The pre-transitional effect may take place. This effect will cause RM grating losing its anisotropic property. Moreover, the grating structure made by free flowing method is not the ideal shape and the variability directly influences the diffraction efficiency. Generally speaking, flow induced method can be utilized of fabricating diffractive grating and create an orientation order for molecules. However, there is still a great improvement space for an ideal DOE.

<div align="right">

Chapter 5

Conclusions

</div>

5.1 Conclusions

A novel fabrication process of forming polymer grating with molecular orientation in LCPG device has been demonstrated in this thesis. The principle of process is that RM monomers can be oriented by weak capillary flow and fixed its order by photo-polymerization. Anisotropic polymer gratings can be formed by way of free flowing process. In recent year, many kinds of phase gratings were studied. Cost down, easy fabrication, high efficiency and polarization independence are the purpose we look for. However, conventional fabrication methods suffered from several drawbacks such as poor separation quality, shrinking effect, long process time, and fringing field problem. Compared with the conventional process, no phase separation, no fringing field, rapid fabrication process can be achieved by our proposed novel process. Nevertheless, some issues of this proposed process were discussed in Chapter 4. In our experiment, the optimizations are still necessary.

5.2 Future Works

LCPGs can be successfully fabricated by the proposed process. But the results of flow alignment and grating shape need to be improved. In order to achieve less defects and more light efficiency devices, the fabrication process need to be further studied in the future.

In order to optimize the structure profile of phase gratings, we need more beautiful PR grating structures. To get defect free alignment, it is helpful to produce uniform micro-channel to confine the depth of RM grating. Besides, a steady pressure source can provide RM flow at a stable velocity that can prevent the perturbation motion. On the other hand, choosing matched materials also can help improving the tuning efficiency of LCPG and eliminate the diffraction phenomenon caused by the mismatch of refractive indices at voltage off state.
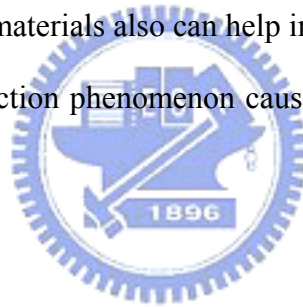
Reference

1. GJ Swanson and Lincoln Laboratory, "Binary Optics Technology: The Theory and Design of Multi-level Diffractive Optical Elements", (Massachusetts Institute of Technology, Lincoln Laboratory, 1989)

2. J. R. Leger, D. Chen and Z. Wang, Opt. Lett. **19**, 108 (1994)

3. P. G. de Gennes, "The physics of liquid crystals", (Clarendon Press Oxford, 1974)

4. M. J. Stephen and J. P. Straley, Reviews of Modern Physics **46**, 617 (1974)

5. Tim Sluckin, David Dunmur and H. Stegemeyer, "Crystals that flow :classic papers from the history of liquid crystals", (Taylor & Francis, London, 2004), p. 738.

6. Ingo Dierking, "Textures of liquid crystals", (Wiley-Vch, Weinheim, 2003), p. 218.

7. A. D. MacNaught, A. Wilkinson and International Union of Pure and Applied Chemistry, "Compendium of chemical terminology: IUPAC recommendations", (Blackwell Science, 1997)

8. I. C. Khoo and S. T. Wu, "Optics and Nonlinear Optics of Liquid Crystals", (World Scientific, 1993)

9. S. T. Wu, U. Efron and L. D. Hess, Appl. Opt. **23**, 3911 (1984)

10. D. W. Berreman, J. Opt. Soc. Am. **62**, 502–510 (1972)

11. R. C. Jones, J. Opt. Soc. Am. **31**, 488–493 (1941)

12. JD Jackson and R. F. Fox, American Journal of Physics **67**, 841 (1999)

13. N. Konforti, E. Marom and S. T. Wu, Opt. Lett. **13**, 251 (1988)

14. M. Schadt and W. Helfrich, Appl. Phys. Lett. **18**, 127 (1971)

15. Karl A. Crandall, et al., Appl. Phys. Lett. **64**, 1741 (1994)

16. J. Chen, et al., Appl. Phys. Lett. **67**, 2588 (1995)

17. C. M. Titus and P. J. Bos, Appl. Phys. Lett. **71**, 2239 (1997)

18. DP Resler, et al., Opt. Lett. **21**, 689–691 (1996)

19. D. Subacius, et al., Appl. Phys. Lett. **71**, 3323 (1997)

20. BH Soffer, et al., Mol.Cryst.Liq.Cryst **70**, 145–161 (1981)

21. I. Fujieda, Appl. Opt. **40**, 6252 (2001)

22. M. Honma and T. Nose, Jpn.J.Appl.Phys. Part 1, 6992 (2003)

23. H. Sakata and M. Nishimura, Jpn.J.Appl.Phys. Part 1, 1516–1521 (2000)

24. R. L. Sutherland, et al., Appl. Phys. Lett. **64**, 1074 (1994)

25. J. Qi, et al., Appl. Phys. Lett. **82**, 1652 (2003)

26. Hongwen Ren, Yun-Hsing Fan and Shin-Tson Wu, Appl. Phys. Lett. **82**, 3168 (2003)

27. Anup K. Ghosh, et al., J. Appl. Phys. **95**, 5241 (2004)

28. Anup K. Ghosh, et al., J. Appl. Phys. **96**, 5909 (2004)

29. Dirk J. Broer, Jan Boven, Grietje N. Mol,Ger Challa, Die Makromolekulare Chemie **190**, 2255 (1989)

30. TJ BUNNING and F. H. KREUZER, Trends in polymer science(Regular ed.) **3**, 318 (1995)

31. DJ Broer, J. Lub and GN Mol, Nature **378**, 467 (1995)

32. J. Lub, P. van de Witte, C. Doornkamp, J.P.A. Vogels,R.T.Wegh, Adv Mater **15**, 1420 (2003)

33. Kohki Takatoh, "Alignment technologies and applications of liquid crystal devices", (Taylor & Francis, London, 2005), p. 263.

34. R. Yamaguchi and S. Sato, Jpn.J.Appl.Phys **35**, L937 (1996)

35. T. Sasaki, H. Fujii and M. Nishikawa, Jpn.J.Appl.Phys **31**, L632 (1992)

36. RJ Atkin, Archive for Rational Mechanics and Analysis **38**, 224 (1970)

37. W. Helfrich, Phys. Rev. Lett. **23**, 372 (1969)

38. JT Jenkins, Annu. Rev. Fluid Mech. **10**, 197 (1978)

39. Miesowicz M, Nature **158**, 261 (1946)

40. D. Demus, JWG Goodby and GW Gray, "Handbook of liquid crystals Vol. 2A", (Wiley-VCH, 1998), p. p 198.

41. D. Grecov and A. D. Rey, Physical Review E **68**, 061704 (2003)

42. D. Grecov and A. D. Rey, J. Non Newtonian Fluid Mech. **139**, 197 (2006)

43. MT Gale, J. Kane and K. Knop, J.Appl.Photogr.Eng **4**, 41 (1978)

44. D. L. White and G. N. Taylor, J. Appl. Phys. **45**, 4718 (1974)